Integrated Master in Bioengineering

Photosynthetic efficiency and CO_2 mitigation by *Phaeodactylum tricornutum* in industrial reactors

Dissertation for Master Degree in Bioengineering
Branche of Biological Engineering

Faculdade de Engenharia da Universidade do Porto – Departamento de Engenharia Química

José Pedro Marques Quelhas

Porto, September 2017

Supervisor: Manuel Simões (FEUP)

Joana Silva (ALGAFARM)

Co-supervisor: Hugo Pereira (ALGAFARM)

"Imagination is more important than knowledge.

Knowledge is limited. Imagination encircles the world."

Albert Einstein

Table of Contents

List of Tables

List of Figures

Acknowledgements

This work would have been much more difficult without the people who are close to me.

First of all, I would like acknowledge all the group that works in ALGAFARM, all the fantastic team that started the ALGAFARM UI&D that were my close colleagues: Hugo, Mafalda, Joana, Adriana, Inês and Pedro.

To Professor Manuel Simões that deeply marked my Bioengineering course, even at the moment of choice of the branch. To him I am really grateful for the guidance and availability of time. Along with Joana Silva who always guided me closely on the field and gave me this internship opportunity.

An acknowledge to my family who always supported me and encouraged me to start this challenge. To Luciana who supported me on the way to Leiria and was my support in the conclusion of the dissertation. Without forgetting the friends, including Luciana, who allowed to disconnect from the dissertation in some moments.

This work was in part funded by projects (i) POCI-01-0145-FEDER-006939 (Laboratório de Engenharia de Processos, Ambiente, Biotecnologia e Energia, UID/EQU/00511/2013) - funded by FEDER through COMPETE2020 - Programa Operacional Competitividade e Internacionalização (POCI) – and by national funds through FCT - Fundação para a Ciência e a Tecnologia and (ii) NORTE-01-0145-FEDER-000005 – LEPABE-2-ECO-INNOVATION, funded by FEDER - Fundo Europeu de Desenvolvimento Regional, through COMPETE2020 – Programa Operacional Competitividade e Internacionalização (POCI) and Programa Operacional Regional do Norte (NORTE2020).

Nomenclature

ALA	Octadecatrienoic/ α-linolenic acid	C18:3 ω-3
ARA	Eicosatetraenoic/ arachidonic acid	C20:4 ω-6
Des	Enzyme desaturase	
DGLA	Eicosatrienoic acid	C20:3 ω-6
DHA	Docosahexaenoic acid	C22:6 ω-3
DPA	Docosapentaenoic acid	C22:5 ω-3
Elo	Enzyme elongase	
EPA	Eicosapentaenoic acid	C20:5 ω-3
FA	Fatty acids	
FAME	Fatty acid methyl esters	
GHG	Greenhouse gases	
GLA	Octadecatrienoic/ ɣ-linolenic acid	C18:3 ω-6
GWP	Green wall panel	
K_La	volumetric CO_2 transfer coefficient	
LA	Octadecadienoic/ linoleic acid	C18:2 ω-6
MUFA	Monounsaturated fatty acids	
PBR	Photobioreactor	
PCDD/F	Polychlorinated dibenzodioxins and polychlorinated dibenzofurans	
PUFA	Polyunsaturated fatty acids	
SDA	Octadecatetraenoic/ stearidonic acid	C18:4 ω-3
SFA	Saturated fatty acids	
TAG	Triacylglycerol	
TCA	Tricarboxylic acid	

Measuring units

A	area	m^2
DW	dry weigh	$g\ L^{-1}$
HHV	higher heating value	$kj\ g^{-1}$
I	irradiance	$\mu Einstein\ m^{-2}\ s^{-1}$
K_I	half saturation constant of irradiance	$\mu Einstein\ m^{-2}\ s^{-1}$
P	volumetric productivity	$g\ L^{-1}day^{-1}$
Pa	areal productivity	$g\ m^{-2}day^{-1}$
$P_{s/X}$	Productivity of extracellular organic carbon	$g\ g^{-1}$
r_x	growth rate	$g\ L^{-1}day^{-1}$
t	time	h
TOC	total organic carbon	$mg\ L^{-1}$
V	volume	m^{-3}
X	biomass concentration	$g\ L^{-1}$
μ	specific growth rate	h^{-1}
μ_{max}	kinetic coefficient of maximum growth rate	h^{-1}

Abstract

After the industrial revolution, there was an increase in the release of greenhouse gases, where CO_2 represents 68% of gases that cause global warming (Pires et al. 2012; Bhola et al. 2013; Waters et al. 2016). Almost all of the countries are trying to reduce this gas emission to approach the past balance of CO_2 (Sayre 2010; Robbins 2016). One of the most promising venues to mitigation of CO_2 is the use of microalgae that are a highly diverse group of photosynthetic organisms (Pires et al. 2012; Jaubert et al. 2017) and responsible for more than 40% of the global carbon capture in the natural world (Hannon et al. 2010). This approach is the option that SECIL has been testing on their facilities since 2010 (SECIL 2017).

Hiper-CO_2-tolerant strains of microalgae are crucial for effective CO_2 mitigation and brackish waters are ideal to find these species (Bhola et al. 2013). *Phaeodactylum tricornutum* can grow in brackish water, making it a potential efficient CO_2 sequester (De Martino et al. 2007; Bhola et al. 2013). This microalgae can be found in planktonic stage with triradiate and fusiform morphologies or in benthonic stage with oval and round morphologies (De Martino et al. 2011).

This microalga has some interesting metabolites, such as carotenoids, phytosterols, vitamins and antioxidants that could be used as supplements for human diet (Gügi et al. 2015). Fucoxanthin is a high-value product that is produced by this microalga with health benefits (Mikami & Hosokawa 2013; Hualian et al. 2015). Furthermore, this species has an interesting lipid profile with a great amount of polyunsaturated fatty acids (PUFA), including the omega 3 fatty acid and omega 6 fatty acid, being EPA the most produced PUFA (Hamilton et al. 2016).

In 5 L airlift reactors, *P. tricornutum* grew at the same level in salinity range between 2.5 and 20 g L^{-1}. The cultures at salinity of 2.5 g L^{-1} showed less percentage of lipids than at 20 g L^{-1}. Although they have similar percentage of EPA, DHA and SDA

represent a lower percentage PUFA that are increased in cultures grown at salinity of 2.5, 5 and 10 g L^{-1}.

In an industrial microalgae production facility of ALGAFARM – Pataias, the 125 L green wall panel (GWP) achieved the maximum cell concentration. The photobioreactor with better volumetric productivity is the 2500 L tubular PBR with 0.235 g L^{-1} day^{-1}. Although the maximum areal productivity was of 45.0 and 48.5 g m^{-2} day^{-1} in 10000 L and 35000 L PBR, respectively without statically significant differences.

The industrial PBR are the most photosynthetic efficient with 2.08% in a 10000 L and 2.21% in a 35000 L tubular PBR. A larger volume in the same area increases the efficiency of the industrial reactors and increasing its height results in a bigger photic region. The biochemistry of industrial biomass is similar to the biochemistry cultured at 20 g L^{-1} at lab scale.

Comparing the benthic and planktonic, these two cultures are very different in terms of biochemical macromolecules. The percentage of protein decreases in benthic morphology, as do the lipids, with a consequential increase in carbohydrates. The increase of carbohydrates is the result of extracellular polymeric matrix of benthic culture.

After determination of stoichiometric equation for *P. tricornutum* growth in 10000 L PBR we can conclude that a fixed value of 2.3 CO_2 gram per gram of biomass is formed. In a 10000 L PBR, the CO_2 sequestration efficiency was 60%. However, in the large PBR the efficiency decreases to 41%. The mixture of biomass and gas, and consequently the contact of these two components, is lower in the 35000 L PBR reducing fixing efficiency.

Keywords: Salinity; Microalgae; CO_2 sequestration; Photobioreactors; *Phaeodactylum tricornutum*; Photosynthesis efficiency; Biomass productivity; Industrial production

Resumo

Após a revolução industrial existiu um aumento da libertação de gases com efeito de estufa, de entre os quais o CO_2 representa 68% dos gases que causam o aquecimento global. (Pires et al. 2012; Bhola et al. 2013; Waters et al. 2016). A maioria dos países estão comprometidos em reduzi r a emissão destes gases para alcançar o balanço natural do CO_2 (Sayre 2010; Nations et al. 2016). Uma das resoluções mais promissoras é a fixação com o crescimento de microalgas que são dos organismos fotossintéticos com maior diversidade (Pires et al. 2012; Jaubert et al. 2017), e responsáveis por 40% da fixação global de carbono (Hannon et al. 2010). Esta é solução que a SECIL está a testar nas suas infraestruturas desde 2010 (SECIL 2017).

Espécies híper tolerantes ao CO_2 são cruciais para melhores resultados de fixação e as águas salobras são as ideias para encontrar estas espécies (Bhola et al. 2013). *Phaeodactylum tricornutum* pode ser encontrado em água salobra, fazendo dele uma espécie com potencial para sequestrar CO_2 (De Martino et al. 2007; Bhola et al. 2013). Esta microalga pode ser encontrada em fase planctónica, com os morfologias de triradiate e fusiforme, e bentónica, com células ovais e redondas (De Martino et al. 2011).

P. tricornutum tem metabolitos interessantes como carotenoides, fitoesteroides, vitaminas e antioxidantes que poderão ser usados como suplementos para alimentação (Gügi et al. 2015). A fucoxantina é um produto de elevado valor acrescentado que é produzido por esta microalga com efeitos benéficos na saúde (Mikami & Hosokawa 2013; Hualian et al. 2015). Além de que esta espécie tem uma perfil de ácidos gordos interessantes, com uma grande percentagem de ácidos gordos insaturados (PUFA), incluindo ácidos gordos ómega 3 e 6, sendo o EPA o mais produzido dos PUFA (Hamilton et al. 2016).

Neste projeto, foi estudado o crescimento deste microrganismo em reatores de suspensão de ar de 5 L crescendo sem diferenças no intervalo de salinidades entre 2.5 e

20 g L^{-1}. A cultura de 2.5 g L^{-1} de sal teve um decréscimo da percentagem de lípidos em relação à crescida a 20 g L^{-1}. Contudo, todos os ensaios tiveram uma percentagem de EPA semelhante, o DHA e SDA foram PUFA em menor percentagem presentes nas salinidades 2.5, 5 e 10 g L^{-1}.

Nas instalações de produção de microalgas da ALGAFARM – Pataias, os reatores de parede verde atingiram maiores concentrações celulares. Os fotobioreaores (PBR) com melhor produtividade volumétrica foram os de 2500 L com 0.235 g L^{-1} dia^{-1}. Porém, a produtividade máxima areal foi de 45.0 e 48.5 g m^{-2} dia^{-1} em PBR de 10000 L e 35000 L, respetivamente, sem diferenças significativas.

Os PBR industriais foram os mais eficientes fotossinteticamente com 2.08% no PBR de 10000 L e 2.21% no de 35000 L. Um volume maior na mesma área de terra ocupada torna reatores industriais mais eficientes.

A bioquímica da biomassa dos reatores industriais foi semelhante à cultivada à escala laboratorial com 20 g L^{-1} de sal. Comparando a cultura bentónica com a planctónica, estes dois estados são muito diferentes a nível bioquímico, ocorrendo um aumento de hidratos de carbono (HC) com a redução percentual das outras biomoléculas. O aumento dos HC é resultado da produção de polímeros extracelulares da matriz.

Após a determinação da estequiometria do crescimento de *P. tricornutum* num PBR de 10000 L conclui-se que este fixou 2.3 gramas de CO_2 por grama de biomassa formada. No PBR de 10000 L, a eficiência de sequestração de CO_2 é de 60%, contudo, no PBR maior a eficiência desceu para 41%. A mistura da fase da biomassa com o gás, e consequentemente o contato destes dois componentes, é foi no PBR de 35000 L, reduzindo a eficiência de sequestração.

Palavras chave: Salinidade; Microalgas; Sequestração de CO_2; Eficiência fotossintética; Fotobioreatores; *Phaeodactylum tricornutum*; Produtividade em Biomassa; Produção industrial

1 Introduction

1.1 Thesis organization

The present work is inserted in the dissertation project to conclude the master's degree in Bioengineering. In this project, the growth of *Phaeodactylum tricornutum* was studied at an industrial scale and the efficiency of this microalga to sequester CO_2 in industrial photobioreactors at ALGAFARM. This dissertation is organized in four major chapters.

The present chapter, one, presents the central problem of climatic changes and ways forward to mitigate this problem. Additionally, this chapter contains a short literature review about microalgae cultivation methods and on some value-added compounds they produce, ways to enhance the production of the metabolites of interest, followed by a presentation of the microalgae under study (*P. tricornutum)* and the company where the project was developed.

Chapter two presents the specification of culture conditions, methods used for the analyses of produced biomass and the statistical analyses of the assays developed.

The third chapter shows the efficiency of growth of this microalga under different salinities and the changes at biochemical level, besides the growth of this alga on different culture volumes, including large scale industrial photobioreactor, as well as the biochemical analyses of the biomass produced and the differences between plaktonic and benthonic stage. This chapter finishes with a stoichiometric analysis of *P. tricornutum* and the efficiency of CO_2 sequestration.

General conclusions and perspectives for future work are discussed in chapter four.

1.2 Problem

Our planet is experiencing a serious climatic change, in which Humans have a significant role. In 2002, the term of "Anthropocene" surges as a recently geological epoch of Earth (Malm & Hornborg 2014). Primarily, when the human civilizations expanded over the planet, they started with the natural manipulation of vegetal species on agriculture, and after by using livestock (Malm & Hornborg 2014; Waters et al. 2016).

The next important step on evolution was the discovery and control of fire, this was the moment when energy trap in detrital carbon started to be used to the primordial interest of this species (Malm & Hornborg 2014). In the 18th century humanity the use of energy on fuel to produce work was already established, which resulted in the beginning of the industrial revolution (Malm & Hornborg 2014; Waters et al. 2016). In the 20th century, population growth increased industrialization that resulted in the intensification of mineral and energy use (Waters et al. 2016).

Further, humans are responsible for an extensive deforestation. This and all previously mentioned activities are the cause of the increased release of greenhouse gases (GHG). The most important molecule in this group is carbon dioxide (CO_2) corresponding to a portion of 68% of GHG that cause the global warming (Pires et al. 2012; Bhola et al. 2013; Waters et al. 2016). In the past, this molecule had a soft balance between the release by biological activities and geological phenomenon versus capture by photosynthesis or adsorption on soil or ocean (Sayre 2010). However, the concentration at the atmospheric level rose from 280 ppm in 1750 to 406 ppm, registered in 2016 (Singh & Ahluwalia 2013; Waters et al. 2016; Isabel & Martins 2017). In 1997, most countries signed the Kyoto protocol which had the objective of reducing GHG by 5.6% against 1990 emission levels. Nowadays, the majority of countries is trying to reduce CO_2 emissions in order to reach zero emissions of GHG's as agreed with the

COP21, that has the ambition to take down global temperature 2 ºC above that of pre-industrial era (Nations et al. 2016).

SECIL is a Portuguese cement company responsible for 37% of the national market, it has activity in a traditional polluting industry, however, the company has the objective of reducing GHG emissions (SECIL 2017).

A polluting industry could try to reduce CO_2 emission as an international obligation, although to reach zero path it would be needed to sequester the CO_2 over a very long geological time. An alternative hypothesis is the direct injection on geological formations or the deposition on ocean as a way to mitigate CO_2 (Pires et al. 2012). Another pathway is to sequester this gas by producing photosynthetic biomass, that allows to sequester for a long geological time (Sayre 2010; Pires et al. 2012). Marine microalgae are responsible for more than 40% of the global carbon capture (Hannon et al. 2010), and are currently considered one of the most promising venues for industrial mitigation of CO_2. This approach is the option that SECIL has been testing on their facilities since 2010 (Pires et al. 2012; SECIL 2015).

1.3 Microalgae

Microalgae are a highly diverse group of photosynthetic organisms and the main producers of marine biomass (Jaubert et al. 2017). It is predicted that between one and ten million of algae exist and most of them are microalgae (Mutanda et al. 2011). These microorganisms display faster growth rates than terrestrial plants, a CO_2 fixation efficiency 10 to 50 times better and with an efficient use of solar power 10 times better (Pires et al. 2012; Bhola et al. 2013). These facts explain why microalgae can produce more 2-10 biomass per land surface area than the most productive terrestrial plants (Sayre 2010).

Hiper-CO_2-tolerant strains of microalgae are crucial for effective CO_2 mitigation, some of these are influenced by environmental factors. Brackish waters are the ideal to find these strains, where there is an high amount of dissolved salts, CO_2 and O_2 (Bhola et al. 2013). The success for production of any microalga with good productivities is their adaptation to the local environment (Mutanda et al. 2011).

Microalgae are rich in various minerals, vitamins, oils and fatty acids (FA), as well as interesting value-added metabolites (Bhola et al. 2013).

The diversity of microalgae is somewhat related to the existence of diverse environments. Diatoms is the major diverse group of microalgae, about 100000 species have been reported, leaving the green algae as the second major group with 8000 species (Mutanda et al. 2011).

Diatoms are among the most productive and flexible group, and have been reported to be responsible for 20% of CO_2 global capture and more than 40% of primary production on the oceans being the major player in carbon cycle (Hildebrand et al. 2012).

CO_2 sequestering is a consequence of the photosynthetic process, the energy captured by light is dissipated by photosystem II, primarily in light-harvesting complex II by thermal dissipation or conduced as the electrons by successive acceptors until CO_2 (Hildebrand et al. 2012). Unlike green algae, diatoms have a xanthophyll-based cycle that increases the efficiency of photosynthesis by reducing the flow of electrons to secondary process (Hildebrand et al. 2012). Diatoms do not have a α-carotene biosynthesis pathway, leading to photoprotective and light harvesting pigments from the same precursor (Hildebrand et al. 2012).

Diatoms, like other groups of microalgae, have the first enzyme of fixation of CO_2 in the form 1D RubisCO that is more efficient than the one present in chlorophytes (Hildebrand et al. 2012; Taucher et al. 2015). This enzyme of photosynthesis is restricted

on subtract to CO_2 and has a lower efficiency, although this species of inorganic carbon has a low concentration on water (Hildebrand et al. 2012; Taucher et al. 2015). So, photosynthetic cells must concentrate CO_2 intracellularly to increase the photosynthetic efficiency. The mechanism of carbon concentrating varies greatly between groups of microalgae, however, it, most of all, converges in the uptake of CO_2 or/and HCO_3^- inside the cells. Carbonic anhydrase has the function of increasing the velocity of conversion of other inorganic carbon into CO_2 to a more extensive reaction of fixation (Taucher et al. 2015). This microalgae has a very regulated uptake system of carbon, that results on no changes in growth rate under different CO_2 pressures, within saturated concentrations (Taucher et al. 2015).

This group of brown microalgae can fix carbon by C3 or C4 metabolism and has a cycle of urea to regulate internal species of inorganic carbon (Hildebrand et al. 2012). In contrast with other microalgae, diatoms have Entner-Doudoroff pathway linked to complete second half of glycolysis in the mitochondrion (Valenzuela et al. 2012).

The main reserve carbohydrate of this algae is chrysolaminarin, a complex carbohydrate with monomers of glucose linked β(1→3) and β(1→6) in a ratio of 11:1. This polysaccharide is soluble and is stored in the chrysolaminarin vacuole, that can be quite large, reaching 50% of cell volume (Hildebrand et al. 2012).

Depending on the conditions of growth or stress they are subjected by the environmental, they produce some specific pigments and proteins as primary metabolites whose metabolic response is known. Secondary metabolites were usually unpredictable although interesting bioactive compounds could be synthetized but had to be discovered empirically (Prestegard et al. 2015).

1.4 *Phaeodactylum tricornutum*

Recently, *P. tricornutum* was accepted as a model organism for the study of diatoms (Prestegard et al. 2015). *P. tricornutum* genome has already been sequenced (Bowler et al. 2008). This organism can grow in brackish water, making it a potential efficient CO_2 sequester (De Martino et al. 2007; Bhola et al. 2013).

This diatom can have four morphologies: triradiate, fusiform, oval or round; a strain isolated in Canada has near 100% of cells in triradiate (De Martino et al. 2007; De Martino et al. 2011).

The change of morphology is a response to environmental factors like temperature or salinity, but genetic information of the strain is important to define the condition necessary to change and the dominant morphology under the environmental conditions in which the strain was collected (De Martino et al. 2007).

The silicified cell wall was not observed in triradiate and fusiform morphology. However, in oval form they are usually seen; this structure is similar to these observed in others diatoms, remains of frustule appear to be observed in fusiform and triradiate (De Martino et al. 2007). When grown in artificial sea water without silica, no significant differences of proportion of morphologies on culture were observed, although the triradiate and oval forms grew significant slower (De Martino et al. 2007). The addition of silicate acid did not change the proportion of morphologies (De Martino et al. 2007). Previous reports had reported silica in organic matrix of fusiform and triradiate, however, it was not proved whether that is a solid siliceous structure or an amorphous form of silica deposited in the matrix of polysaccharides (Johansen 1991). Before, it was verified by electron micrograph that fusiform was devoid of solid siliceous wall (Lewin et al. 1958).

Oval form resist better to low radiation or nutrients deficiency, and other morphologies are dominant in the starting of batch rise the proportion of oval cells in this

conditions, these tend to aggregated in a cluster with some round cells (De Martino et al. 2007).

P. tricornutum has its normal growth on autotrophic conditions, but to increase the productivity and come to higher levels of biomass concentration (like increases of 30%), they can be grown in mixotrophic conditions with supplementation of glycerol (Morais et al. 2009). Some strains of this microalga can transport into the cell glucose, and grow in the presence of light with different efficiencies (Liu et al. 2009). Reported heterotrophic growth of this diatom was already reported, by means of genetic improvement of the species (Ceron Garcia et al. 2006; Hamilton et al. 2016).

As commonly described in other microalgae, under nitrogen and/or phosphate starvation, *P. tricornutum*, intensifies the lipid amount per cell, with a partial turnover of carbohydrates (Valenzuela et al. 2012; Longworth et al. 2016). Under these conditions the recycling of intracellular nitrogen is increased by the over-expression of glutamate dehydrogenase and glutamine synthetises (Valenzuela et al. 2012). Thus, it decreases the expression of light-harvesting complex, thereafter, chlorophyll *a* and fucoxanthin were reported lowering expression (Valenzuela et al. 2012; Longworth et al. 2016).

Under starving the expression of tricarboxylic acid (TCA) genes declines, that results in a minor metabolism velocity. Even though lipids continue to be packed, with increasing expression of FA biosynthesis, triacylglycerol (TAG) assembly, chain modifications, and β-oxidation, these two last groups of enzymes possibly responsible for recycling of some nitrate and phosphate in FA (Valenzuela et al. 2012).

In normal conditions of nutrients, *P. tricornutum* intensifies the sequestration of inorganic carbon by biophysical mechanisms that direct transport of inorganic carbon by the membranes to chloroplast, another path is to fix inorganic carbon by carboxylase to

C3, form a C4 that can be transported to target organelle and from there deliver the inorganic carbon to RubisCO (Valenzuela et al. 2012).

The cells division of this stain is up-regulated by a sensor of radiation on the photoreceptors (Jaubert et al. 2017). The red light and blue light are perceived by different photoreceptors, blue light active the mechanism of Aureo1a and red/far-red light perceived by phytochrome, this leading to a different metabolic pathway, which downstream actors are still unknown. In this complex response is involved the circadian clock to network the photoreceptors and chloroplast-derived signals (Jaubert et al. 2017). The fact of up regulation of cell division by radiation may be a reason for not achieving heterotrophic growth.

Previous reports byPérez et al. (2008) provided the Monod model for radiation factor to *P. tricornutum*:

$$\mu = \frac{\mu_{max}\, I}{I + K_I} = \frac{I \times 0.08\, h^{-1}}{I + 10.2\, \mu Einstein\, m^{-2}\, s^{-1}} \quad (1)$$

Where μ is the specific growth rate, μ_{max} is the kinetic coefficient of maximum growth rate, I is the average irradiance inside the culture and K_I is half saturation constant of irradiance. Which indicates that the increase of light intensity have a maximum growth rate of 0.08 h^{-1} and the half of maximum growth it's at 10.2 μEinstein m^{-2} s^{-1} (Pérez et al. 2008).

This microalga has some interesting metabolites, such as carotenoids, phytosterols, vitamins, and antioxidants that could be used as supplements for human diet (Gügi et al. 2015). Carotenoids are constituted by a linear backbone with 40 carbons and more than 11 conjugated bonds, most of them are colourful and responsible for colour in some animals like orange colour of salmon meat. Although animals do not produce these molecules, they accumulate carotenoids upon ingestion (Mikami & Hosokawa 2013).

P. tricornutum produces fucoxanthin, a high value carotenoid that is interesting because of its health benefits, such as, antioxidant (that is predictable by the presence of conjugated system in the molecule and groups electron accepter like carbonyl group – Figure 1), anti-inflammatory, anti-neoplasic, antidiabetic, antiangiogenic, antimalarial and anti-obesity activities (Mikami & Hosokawa 2013; Hualian et al. 2015; Raposo et al. 2015).

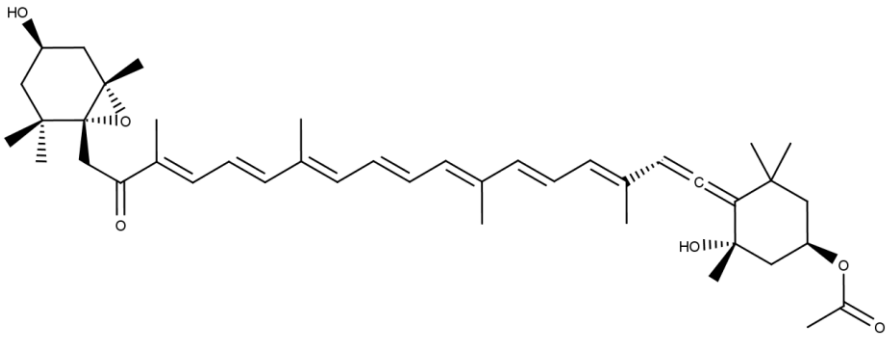

Figure 1 - Two-dimension representation of molecular structure of fucoxanthin (drawn on Marvin Sketch based on Mikami & Hosokawa 2013).

The biosynthesis pathway of fucoxanthin is not fully known. Like green algae they have the pathway to convert β-carotene to neoxanthin, although the absence of specific enzymes to convert neoxanthin to fucoxanthin in the genome of *P. tricornutum*, leads to uncertainty as to what would be the intermediary prior to fucoxanthin: neoxanthin or diadinoxanthin (Mikami & Hosokawa 2013).

Differences on culture medium (nutrients) or radiation imply changes on fucoxanthin production by cells. The depletion of silica reduces the percentage of fucoxanthin inside the cell (Zhao et al. 2014), whereas, nitrogen depletion reduces the productivity of fucoxanthin. Moreover, low temperatures (10ºC) and lower levels of light leads to a greater amount of fucoxanthin than higher temperatures (25ºC) or higher levels of light (15 klux) (Shimura & Fujita 1975). Iron as also a key effect on the fucoxanthin

concentration, 10 μM of iron intensifies the production of fucoxanthin in contrast to lowers concentrations (Kosakowska et al. 2004).

Furthermore, *P. tricornutum* has an interesting lipid profile with great amount of polyunsaturated FAs (PUFA), including the omega 3 fatty acid and omega 6 FAs (Hamilton et al. 2016).

The most produced omega 3 is the eicosapentaenoic acid (EPA, C20:5 ω-3) and with lower percentages of octadecatetraenoic (stearidonic acid, SDA, C18:4 ω-3), octadecatrienoic (α-linolenic acid, ALA, C18:3 ω-3), docosahexaenoic (DHA, C22:6 ω-3) and docosapentaenoic (DPA, C22:5 ω-3) acids (Zhao et al. 2014; Hamilton et al. 2014; Hamilton et al. 2016). Regarding omega 6 PUFA, octadecadienoic (linoleic acid, LA, C18:2 ω-6), octadecatrienoic (ɣ-linolenic acid, GLA, C18:3 ω-6), eicosatetraenoic (arachidonic acid, ARA, C20:4 ω-6) and eicosatrienoic (DGLA, C20:3 ω-6) acids are the most reported (Zhao et al. 2014; Hamilton et al. 2016).

P. tricornutum and others diatoms do not produce the DHA like animals, via the Sprecher pathway by shortening tetracosahexaenoic acid with the recourse to β-oxidation of this FA (Mühlroth et al. 2013). For their side, they have a simpler process using elongation and desaturation of FAs to produce DHA (Mühlroth et al. 2013).

The tricarboxylic acid cycle (in mitochondria) are intermediaries and share the acetil-CoA as primordial precursor of FA synthesis (in chloroplast), the β- oxidation enzymes (in mitochondria) are also involved in the production of FA (Mühlroth et al. 2013). In the presence of oxygen, the saturated FA are unsaturated by desaturases (Des) present on smooth endoplasmic reticulum (Mühlroth et al. 2013). Either, tricarboxylic acid cycle, β-oxidation, FA synthesis, membrane glycerolipid synthesis, PUFA synthesis and Kennedy pathway are involved on synthesis of EPA and DHA (Mühlroth et al. 2013).

The biosynthesis of EPA by *P. tricornutum* are a combined process between both the omega 3 and omega 6 fatty acid pathway, that could be observed in Figure 2 (Khozin-goldberg et al. 2011; Mühlroth et al. 2013; Hamilton et al. 2014).

The improvement of enzyme glycerol-3-phosphate acyltransferase improves the production of PUFA (Niu et al. 2016), and a genetical manipulation of this diatom inserting genes of Δ6–desaturase and Δ5-elongase improves the production of DHA and DPA (Hamilton et al. 2014; Hamilton et al. 2015).

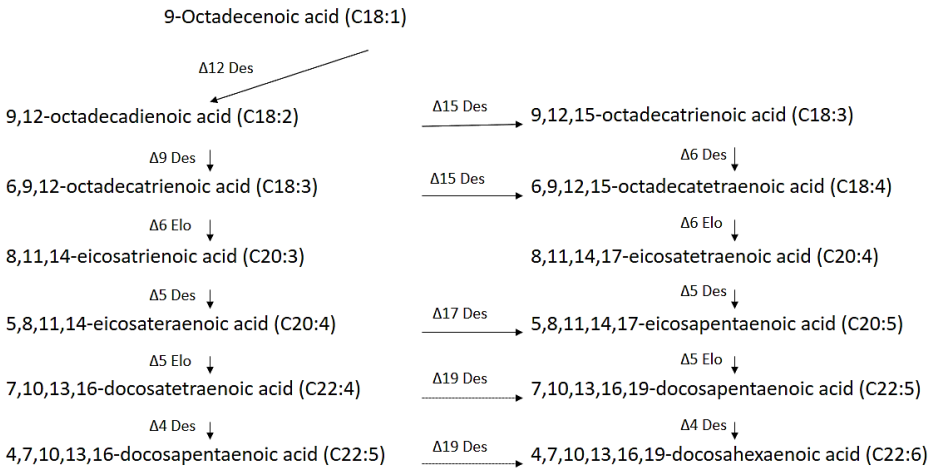

Figure 2- Biosynthesis of EPA and DHA on *P. tricornutum* based on previous reports. Des is enzyme desaturase and Elo is enzyme elongase. (based on: Khozin-goldberg et al. 2011; Mühlroth et al. 2013; Hamilton et al. 2014)

Under sub optimal environmental conditions like low nitrogen concentrations, the production of EPA and incorporation in triglycerides are improved (Yongmanitchai & Ward 1991; Mühlroth et al. 2013).

In the presence of glycerol in the culture medium of *P. tricornutum* an increase in PUFA is observed (Ceron Garcia et al. 2006; Mühlroth et al. 2013). On the other side, the use of ammonia as source of nitrogen inhibits the production of EPA and other FA (Yongmanitchai & Ward 1991; Wen & Chen 2003), although urea is a nitrogen source that improves the *P. tricornutum* growth and rises the productivity on EPA (Yongmanitchai & Ward 1991). The presence of phosphate in the range of 0.1-0.5 g L^{-1}

is important to the yield in omega 3 PUFA (Yongmanitchai & Ward 1991; Wen & Chen 2003).

The percentage of omega 3 PUFA acids decreases with increases of salinity of the medium (Yongmanitchai & Ward 1991; Wen & Chen 2003). When temperature decreases from 25ºC to 10ºC for 12h the result is an increases in the fraction of PUFA, mainly in the form of EPA (Wen & Chen 2003; Sharma et al. 2012).

ARA, EPA and DHA are synthetized by human but with a lower extension, which requires an intake of these FAs, even more important in the primordial phase of life to structural structed of brain membrane phospholipids with ARA and DHA (Mühlroth et al. 2013).

In Western countries it is recommended an increase in omega 3 consumption because the ratio of omega 6 to omega 3 is greater than 15:1, although the recommended ratio for a balanced diet is 4:1 (Mühlroth et al. 2013). Terrestrial plants and their derivatives, and terrestrial animals that feed on these have the ratio omega 6 per omega 3 higher than 4:1 however the microalgae and their consumers have a ratio of 2:1 (Mühlroth et al. 2013).

Omega 6 PUFA have an important role in immunological regulation, with a proinflammatory effect. On the other side, omega 3 PUFA have anti-inflammatory properties, reducing the risk of cardiovascular disease, colorectal cancer, breast cancer and asthma (Swanson et al. 2012; Mühlroth et al. 2013).

Extract of *P. tricornutum* combined with nanofibers mats has antimicrobial activity, and also antifungal and antiviral effects of PUFA have been reported (Desbois et al. 2009; Mühlroth et al. 2013; Kwak et al. 2014).

All the morphologies have been successfully transformed by nanoparticle bombardment and multi-pulse electroporation, with more difficulties associated with

triradiate form (De Martino et al. 2007). Recently, biomolecular products with interest in pharmaceutical applications, such as monoclonal antibodies against hepatitis B, were produced in this strain (Vanier et al. 2015).

1.5 ALGAFARM

SECIL group produces cements and mortars. The main GHG they release as secondary product is CO_2 from calcination of carbonates from raw material (60% of emissions) and combustion of fuel in the ovens (40% of emissions) (SECIL 2017).

This industry also produces NO_x, SO_x and some volatile organic compounds, and in lower levels heavy metals, polychlorinated dibenzodioxins and polychlorinated dibenzofurans (PCDD/F). With a view to attaining a more sustainable production, SECIL has used bag filters, low NO_x burners, selective non-catalytic reduction, systems of control of NO_x and SO_x, this with an injection of lime/calcium hydroxide, and electrostatic particles precipitations for 20 years (SECIL 2017).

Recently, SECIL has reduced the CO_2 emissions by increasing the efficiency of process and co-processing of alternative fuels. Additionally, they started testing the sequestering of CO_2 emissions with recourse to microalgal growth in the facilities of ALGAFARM, showed in Figure 3 (SECIL 2017).

ALGAFARM is the biggest industrial unity producing microalgae in Europe, located in Pataias near Leiria, close to the SECIL cement factory (Fonseca et al. 2016; Silva et al. 2017). The relation with cement factory derive from the use of gas effluents to produce microalgae, more specifically the GHG CO_2 with the main purpose of having a sustainable cement industry (Silva et al. 2017).

Figure 3 – ALGAFARM facilities (fron: Silva et al. 2017).

During 2017, ALGAFARM has demonstrated the possibility of *Chlorella vulgaris* growth in dark heterotrophic conditions, without photic shock when changed the condition of growing to autotrophy in green wall panels (GWP Silva et al. 2017). With this process it was possible to obtain biomass with premium quality with interesting levels of total microorganisms (about 10^2 unities), fungi and yeasts (lower than 10^1), still with biochemistry levels higher than normal *C. vulgaris* powder (Silva et al. 2017).

This premium *C. vulgaris* is produced with the aim of selling for human consumption. *Nannochloropsis* sp. is also produced in ALGARFM. This strains is rich in omega 3 fatty acids, and is commonly used in aquaculture and others feed options. Others strains such as *P. tricornutum*, *Tetraselmis* sp. and *Haematococcus* sp. are also being used in ALGAFARM, at pilot scale (Fonseca et al. 2016; Silva et al. 2017).

Large scale production in ALGAFARM is mainly composed by tubular photobioreactor (PBR). These PBR are inoculated with *C. vulgaris* cultivated heterotrophically in fermentaters with capacities of 200 and 5000 L. This strategy significantly reduces the scale-up time, a constringency frequently reported within the autotrophic cultivation of microalgae (Fonseca et al. 2016; Silva et al. 2017). Several advantages are reported to PBR *i.e*. the capacity to obtain high quality biomass with lower

levels of contamination, the reactor geometry that provides greater productivities versus open-pound, by allowing the growth of more diversity of algal and easily preventing the evaporation of culture medium. On the other hand, this system is more expensive to operate and has a complex process of scale-up (Tredici 2010; Fonseca et al. 2016). The use of PBRs agree with the objective of the sequestering of CO_2, since it is a geometry that allows greater sequestration efficiencies when compared to open systems (Bhola et al. 2013). The photic zone of reactors are constructed with a transparent plastic tube that allow the transference of energy in the form of radiation but prevents mass transfer to the outside (Fonseca et al. 2016).

In 2013, ALGAFARM started to produce *Chlorella* sp. combining the autotrophic with the mixotrophic growth of microalgae. Pre-inoculum was produced in 5 L balloons and the inoculum in GWP of 1 m^3 each. In 2016, the fermentation technology was introduced in ALGAFARM. The next step will be the construction of raceways to produce biomass with lower costs (Silva et al. 2017).

All the data present in this work was collected in this facility between March 6th and July 26th 2017 (period of spring-summer).

2 Materials and Methods

2.1 Microalgae strain and culture medium

All experiments described in the present work were performed at the facilities of CMP/ALGAFARM (Secil Group, Portugal), between the 15th of February and the 15th of August 2017 while the biochemical profile of produced biomass was performed at the MarBiotech group of the Centre of Marine Sciences (University of Algarve) between the 24th and 28th of July 2017. The microalgal strain used in this work, *P. tricornutum*, was obtained from ALGAFARM culture collection. Culture medium was based on Guillards F2 medium adjusted to the local water at pH 8, which was further supplemented with iron (25 μM) and sodium silicate (2 mM).

2.2 Salinity test

For the salinity test, *P. tricornutum* was grown in triplicate at 2.5, 5, 10 and 20 g L^{-1} (control) of salt in 5 L air-lift reactors, until the stationary growth phase was reached. Cultures were maintained with aeration, mixed with filtered air (0.2 μm) and the pH was kept at 7.5-8 by the addition of pulses of CO_2. The reactors were operated with continuous lightning (24h), with an intensity of 6350 Lm, and maintained at 24ºC.

Every two days, cultures were monitored by microscopic observations of culture, salinity analysed by refractometer, measures of the optical density at 540 nm and of the dry weight (DW) of culture (this is further explained in section 2.5).

2.3 Scale-up of cultures for industrial production

Microalgae cultures were scaled-up from 5 L laboratory air-lift reactors under the same aforementioned conditions. Two 5 L reactors were used as the pre-inoculum to grow a 125 L GWP. Figure 4 shows a structural diagram of the 125 L GWP, which was later used to seed a 250 L GWP. GWP were aerated with filtered air (0.2 μm), the pH was kept

between 7.5 and 8 by the addition of pulses of CO_2. The temperature was maintained by a sparkling water system below 28ºC and the air flow of 0.25 v.v.m. (air volumes per volume of reactor per minute).

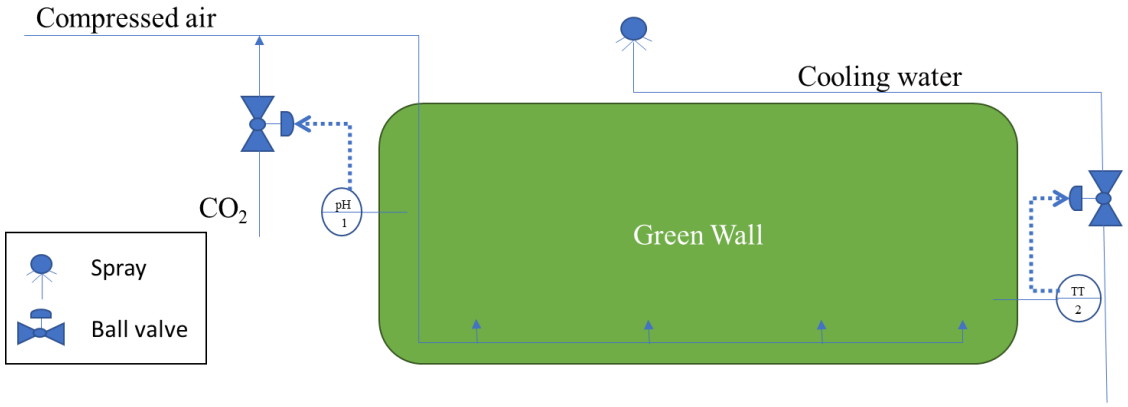

Figure 4 - Pipe and instruments diagram of Green Wall panel. pH is a sensor of pH, TT is a temperature transmitter, solid line represents pipe, and dashed line means a manual regulation.

Two 250 L GWP were used to inoculate a 2500 L tubular (Figure 5). About 80% of this PBR was used as an inoculum to start a 10000 L PBR (Figure 6). The 35000 L PBR started with a culture seed of 80% obtained from the 10000 L PBR.

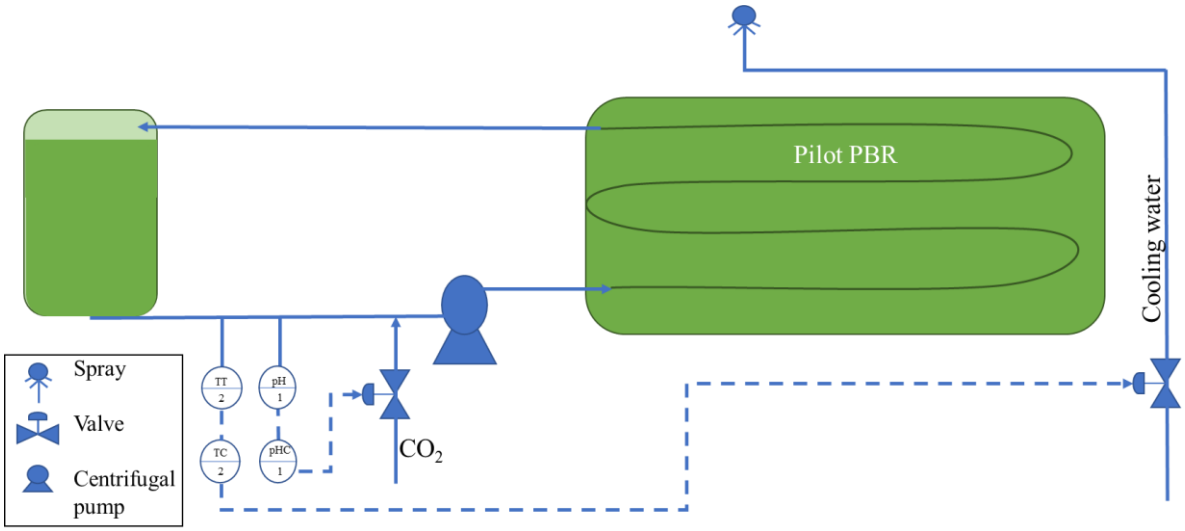

Figure 5 - Pipe and instruments diagram of pilot scale PBR (2500 L). pH is a sensor of pH, TT is a temperature transmitter, pHC is the controller that respond to changes of pH, TC is a controller that take temperature to set point of 28ºC; solid line represent pipe and dashed line means an electric signal to connect.

The tubular PBRs were kept below 28ºC using a sparkling water system and an automatism of CO_2 injection kept the pH below 8, the culture circulates at 1.0; 0,80 and 0.65 m s^{-1} inside the tubes in 2500 L, 10000 L and 35000 L, respectively. GWP and PBR were maintained under a summer circadian photoperiod. The monitoring of culture was done every day, as explained in section 2.5.

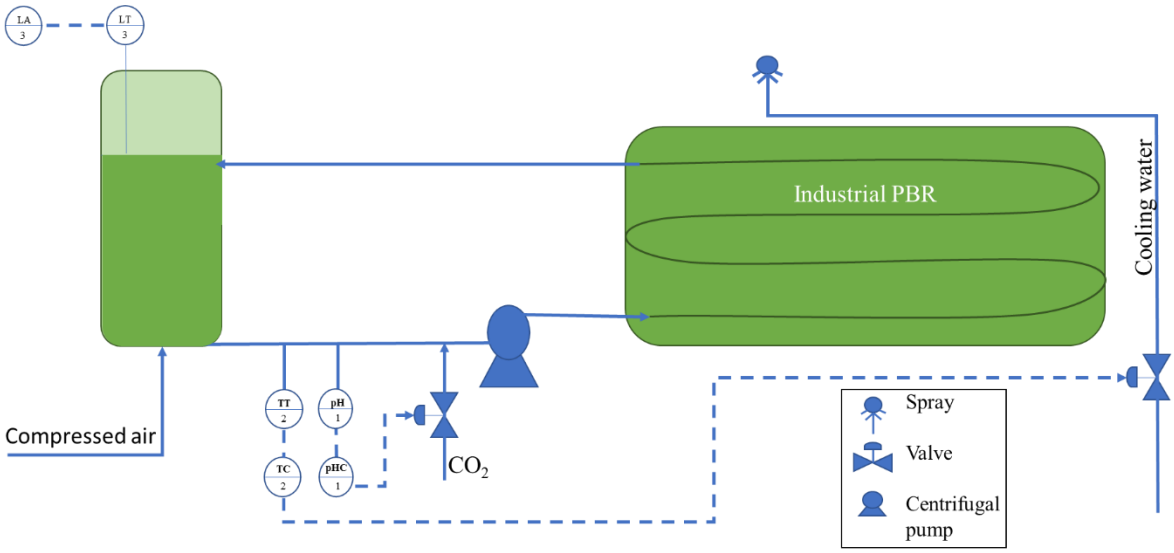

Figure 6 - Pipe and instruments diagram of industrial PBR (10000 L or 35000 L). pH is a sensor of pH, TT is a temperature transmitter, LT is a level transmitter, pHC is the controller that responds to changes of pH, TC is a controller that takes temperature to set point of 28ºC, LA is an alarm that warns when liquid rise or foaming; solid line represents pipe and dashed line means an electric signal to connect.

2.4 Photosynthetic efficiency

The photosynthetic efficiency was assessed by growing three air-lift reactors of 125 L at the same time until the stationary phase was reached. Moreover, three consecutive replicas of 2500 L and 10000 L were grown in the PBR, these reactors were renewed when culture ended the exponential phase, as two successive batch in 35000 L PBR grew to the end of exponential phase. These reactors were grown at salinity of 20 g L^{-1}. The temperature and pH of culture were controlled as described in section 2.3 and monitored according to section 2.5. The outside temperature and solar radiation were measured using a meteorological station (RM Young) and an Apogee Logan UT SP-110 pyranometer.

2.5 Growth assessment

The growth of microalgae cultures was evaluated by optical density and DW (calibration curve of optical density per DW shown in Figure b). Optical density was measured in Genesys 10s UV-Vis spectrophotometer at 540 nm (Reis et al. 1996). DW was determined by filtering a defined volume of a given sample on microglass filters (0.7 µm, VWR), which was further washed with an equal volume of ammonium formiate (37 g L^{-1}) and dried on AND MS-70 moisture analyser (Prestegard et al. 2014).

Volumetric biomass productivity (P) was determined by the division of DW differences in grams per litter (X_1 and X_2) and the time interval (t_1 time of sample of X_1 and t_2 time of sample of X_2).

$$P\ (g\ L^{-1} day^{-1}) = \frac{X_2 - X_1}{t_2 - t_1} \quad (2)$$

Areal biomass productivity (Pa) was determined by multiplying the volumetric biomass productivity by the volume of the PBR in litters (V) and division by the area of PBR, in square meters (A).

$$Pa\ (g\ m^{-2} day^{-1}) = \frac{P \times V}{A} \quad (3)$$

The specific growth rate of culture (µ) was estimated by the quotient between the growth rate (r_x) and the concentrations of biomass (X) at that moment. The development of the integral results in the simplified equation that is the fraction between the Neo-logarithmic of biomass concentration (X_2) on time later (t_2) divided by biomass concentration (X_1) on time previous (t_1) and the time interval (t_2 less t_1).

$$\mu\ (day^{-1}) = \frac{r_X}{X} = \frac{1}{X}\frac{dX}{dt} = \frac{\ln(X_2/X_1)}{t_2 - t_1} \quad (4)$$

The photosynthetic efficiency was determined by the ratio between the increase of higher heating value (HHV) and the sun irradiation that reached the reactor.

The HHV was calculated according to a previous correlation (Callejón-Ferre et al. 2011), where C is the percentage of carbon determined on CHN, H the percentage of hydrogen and N the percentage of nitrogen.

$$\text{HHV (kJ g}^{-1}) = -3.393 + 0.507\ \text{C} - 0.341\ \text{H} + 0.067\ \text{N} \quad (5)$$

2.6 Biochemical composition

The ash content was determined by burning 1 g of biomass in a furnace at 550ºC for 8 hours shown in Figure 7 F (MODEL, BRAND).

Total lipids were determined by previous modified method (Bligh & Dyer 1959) reported by Pereira et al. (2012). Lipids were extracted from the biomass using a mixture of chloroform, methanol and water (2:2:1), homogenised with an Ultra Thurrax at 1600 g for 2 minutes. The lipid extracts were later centrifuged and the chloroform phase was recovered with a Pasteur pipette. A known volume of the chloroform phase was pipetted to pre-weight tubes and evaporated overnight. The dried residue was compared with dried mass of culture to obtain the percentage of lipids. Figures 7 A, B, C, D and E show some steps of the procedure explained.

Total proteins were calculated by multiplying the percentage of nitrogen by 6.25 (Marinho et al. 2017), after CHN determination (Nunez & Quigg 2016) using a Vario el III (Vario EL, Elementar Analyser system, GmbH, Hanau, Germany) according to the procedure provided by the manufacturer. Carbohydrates were determined by the difference between the other principal macromolecules.

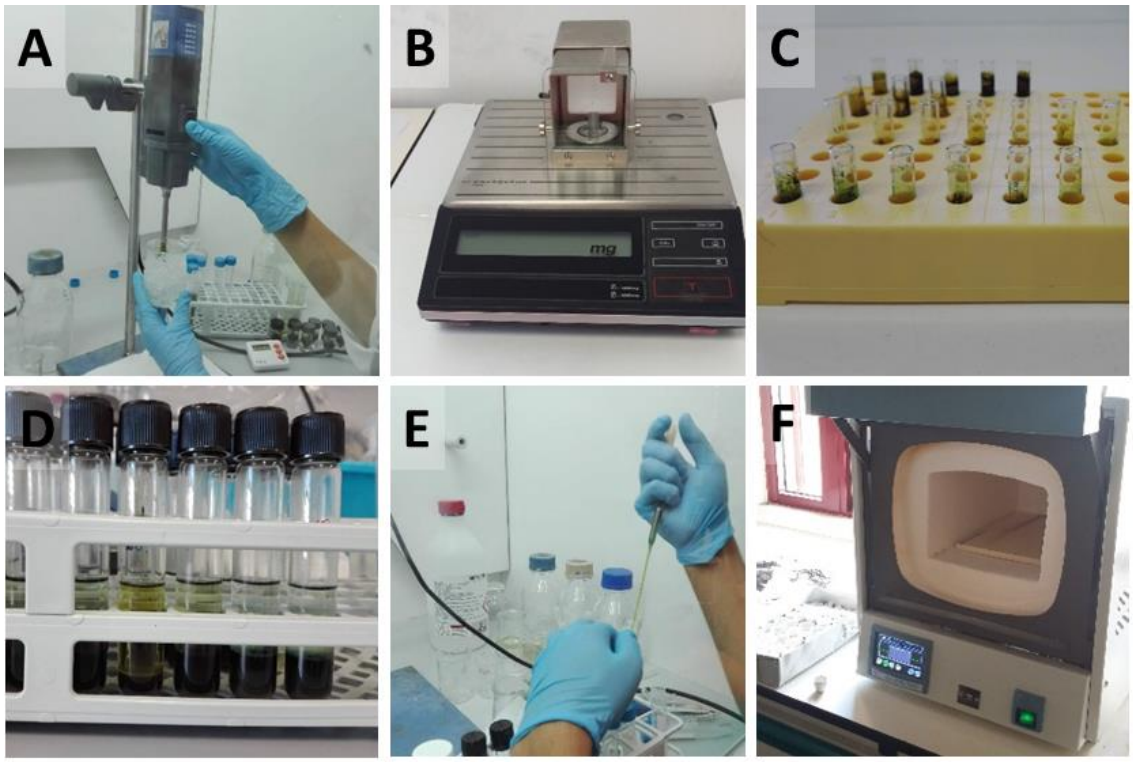

Figure 7 - Some of the steps of lipid quantification and ash determination. (A) lipids extraction on Ultra Thurrax; (B) mass measurement of lipid drying vessels; (C) vessels with the samples dried; (D) lipids extracted with phase separation after centrifugation; (E) removal of chloroform phase with a Pasteur pipette; (F) furnace where the biomass was dried to find the percentage of ash.

2.7 Fatty acids profile: preparation and determination

FA were converted to the corresponding fatty acid methyl esters (FAME) according (Lepage & Roy 1984) protocol modified by Pereira et al. (2012).

FA were derivatized by weighing 0.05 g of freeze dried microalga in reaction vessels. Afterwards, 1.5 mL of a solution containing methanol and acetyl chloride (20:1 v/v) was added and the mixture was homogenised on ice with an Ultra Thurrax (12000 rpm) for 90 seconds. Subsequently, 1 mL of hexane was added and the mixture was heated for 1 hour at 90ºC (Figure 8 C). Then, 1 mL of water was added to the mix and the organic phase was removed to another vessel, dried with anhydrous sodium sulphate and filtered before analyses (Figures 8 D and E).

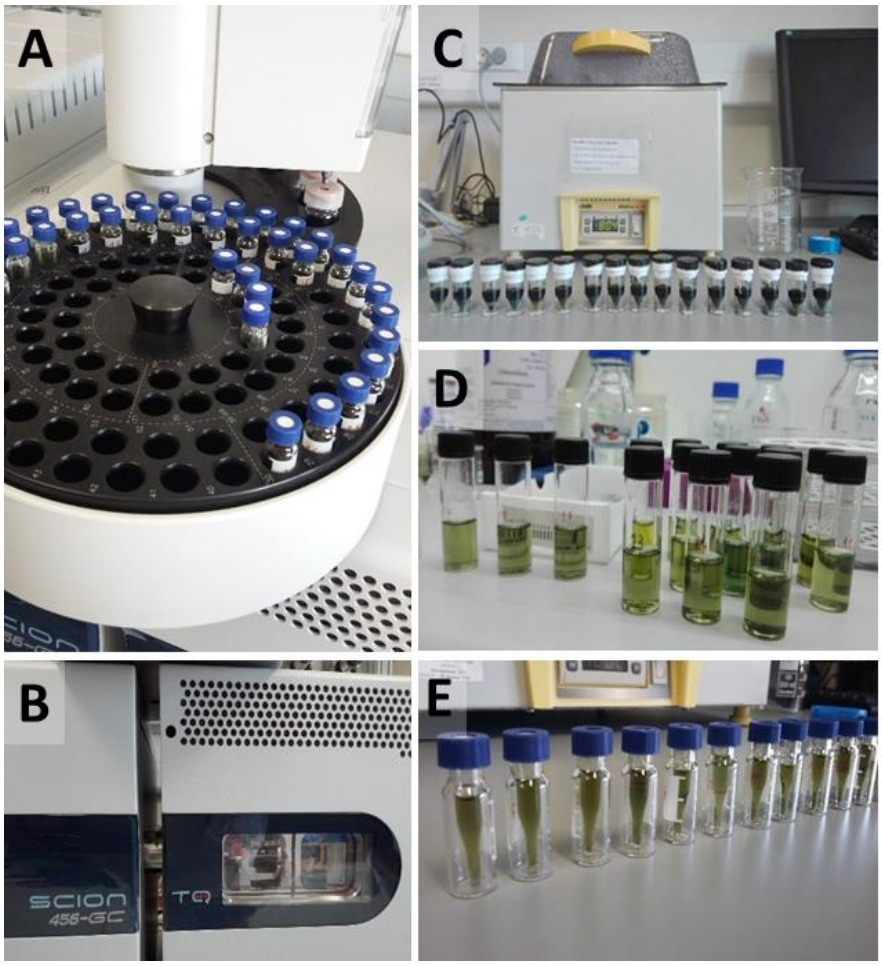

Figure 8 – Some of the steps of fatty acid samples preparation and the apparatus used. (A) the automatized plate of chromatograph; (B) the GC-MS chromatograph analyser; (C) samples before heat treatment during one hour; (D) samples before being treated with anhydrous sodium sulphate; (E) samples ready to be analysed in chromatography.

FAME were analysed in a Bruker GC-MS (Bruker SCION 456/GC, SCION TQ MS) equipped with a ZB-5MS (30 m with 0.25 mm of internal diameter, and 0.25 μm of film thickens, Phenomenex) using helium as carrier gas, (Figure 8 A and B). The temperature program was 60ºC (1 min), with an increase of 30ºC per min up to 120ºC, 5ºC min^{-1} up to 250ºC, and 20ºC min^{-1} up to 300ºC. The temperature in the injector was 300ºC. For identification and quantification of FAME first was analysed five different concentration of Supelco® 37 component FAME Mix (Sigma-Aldrich, Sintra, Portugal) to establish 37 different calibration curves for each of the FAME in the commercial standard. In case of some other FAME not present in standard and was identify by mass

spectrum, the response factor of the most similar FAME was used, in terms of structure. Results are expressed in percentage of total FAME on biomass (Pereira et al. 2016).

2.8 Stoichiometric equation

The essential stoichiometric equation of microalgae in autotrophic condition (Myint et al. 2013), modified with the addition of extracellular compounds represented by a sugar as the major dissolved organic carbon (Granum et al. 2002; Thornton 2014) is present in equation 6:

$$aCO_2 + bNO_3^{2-} + cH_2O + dH^+ \rightarrow fC_wH_xN_yO_z + gO_2 + hHCO_3^- + iH^+ + jC_6H_{12}O_6 \quad (6)$$

Where *w*, *x*, *y* and *z* represent the stoichiometric ratio of each one of the principal elements of biomass: *w* refers to ratio of carbon (C), *x* to ratio of hydrogen (H), *y* to ratio of nitrogen (N), and *z* to ratio of oxygen (O). The percentage in mass of carbon, nitrogen and hydrogen was determined by CHN analyses.

$$w = \frac{\%C/_{atomic\ mass\ C}}{\%C/_{atomic\ mass\ C}} = 1 \quad (7)$$

$$y = \frac{\%N/_{atomic\ mass\ N}}{\%C/_{atomic\ mass\ C}} \quad (9)$$

$$x = \frac{\%H/_{atomic\ mass\ H}}{\%C/_{atomic\ mass\ C}} \quad (8)$$

$$z = \frac{(1 - \%H - \%C - \%N)/_{atomic\ mass\ O}}{\%C/_{atomic\ mass\ C}} \quad (10)$$

The productivity of extracellular organic carbon ($P_{s/X}$) was determined by the quotient between the final concentration of organic carbon (TOC_f) minus the initial concentration of organic carbon (TOC_i) for the difference between the biomass at initial (X_i) and final (X_f) measurements.

$$P_{s/X} = \frac{TOC_f - TOC_i}{X_f - X_i} \quad (11)$$

Furthermore, *a*, *b*, *c*, *d*, *e*, *f*, *g*, *h*, *i* and *j* are the stoichiometric coefficients of these molecules that are involved on the photosynthetic process (carbon dioxide, nitrate, water, proton, biomass, oxygen, hydrogen carbonate, proton and sugar, respectively).

The balance to each one of the elements results in the resolution of the stoichiometric equation of photosynthesis of *P. tricornutum.*

$$\begin{cases} a = wf + h + 6j & (Carbon\ balance) \\ 2a + 3b + c = zf + 2g + 3h + 6j & (Oxygen\ balance) \\ 2c + d = xf + h + i + 12j & (Hydrogen\ balance) \\ b = yf & (Nitrogen\ balance) \\ j = f\left(P_{S/X} \times \dfrac{Biomass\ molar\ mass}{6 \times atomic\ mass\ C}\right) & (Relation\ biomass - TOC) \\ -2b + d = -h + i & (Charge\ balance) \end{cases} \quad (12)$$

2.9 Carbon sequestration

The quantification of sequestered CO_2 was determined considering that the CO_2 concentration dissolved in the medium of culture at the beginning and end of the experiment will be the same if pH and temperature remain the same (Laws et al. 1997). The amount of CO_2 added in culture was registered by placing a rotameter in the injection system and an in-house automatism that collects the data in real time.

The biomass DW was related with the percentage of carbon analysed by CHN and the carbon content of the supernatant analysed by total organic carbon (TOC). The amount of CO_2 sequestered in the biomass was the mass of carbon accumulated by the microalgae biomass during growth.

To determine the TOC dissolved in the culture medium, the supernatant of medium was acidified with sulfuric acid to pH 2 and filtered through glass fiber membrane (1.6 μm, VWR) before being injected on TOC-VCSN-Total Organic Carbon analyser, Shimadzu, with a combustion at 720ºC, the methods have a range of measuring of 0.1 to 4000 mg L^{-1} (Mata et al. 2012).

The sequestered CO_2 is the sum of organic carbon in the form of extracellular organic compounds and the biomass.

2.10 Statistical analysis

Analyses of linear regression, *t student* and multivariable statistic tests were done using SPSS 24.0. When three or more conditions were analysed ANOVA was performed with the multiple comparison of Turkey-HSD and to compare to groups of independent results a *t-student* test was used. A confidence level ≥ 95% was used. For each test, triplicate mean and standard deviation was determined.

3 Results and discussion

3.1 Salinity assay

P. tricornutum grew similarly in all salt concentrations understudy, namely 2.5, 5, 10 and 20 g L^{-1} (Figure 9), without any statistical differences among the treatments ($p \geq 0.05$). *P. tricornutum* has grown exponential for 14 days, at last of 16 days start the stationary phase, in the beginning there was a lag phase for 2 days. The effect of salt on the growth of this strain is strain-dependent, as some previous reports showed an optimum salinity of 20 g L^{-1} (Santos et al. 2002; Liang et al. 2014), as well as 5 g L^{-1} in others (Yongmanitchai & Ward 1991).

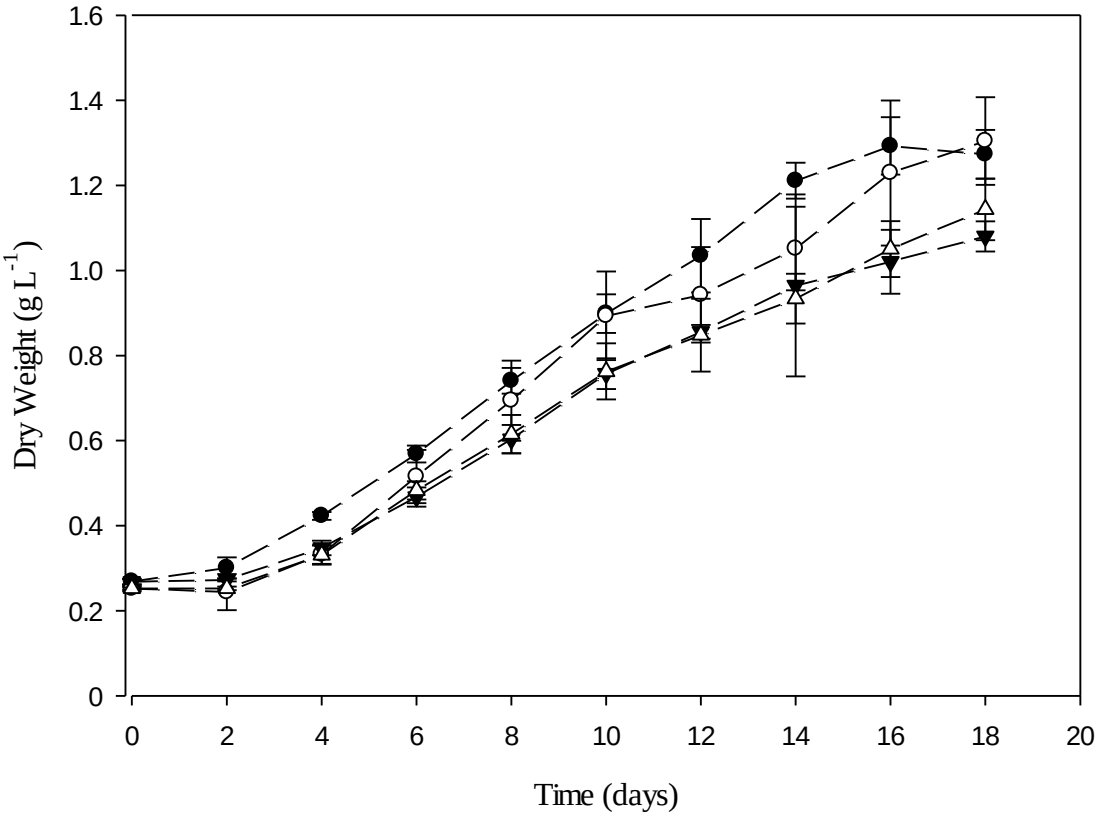

Figure 9 – Batch growth of *P. tricornutum* in 5 L reactors under four different salinities. Dry weight of culture at 20 g L^{-1} (●); at 10 g L^{-1} (○); at 5 g L^{-1} (▼) and at 2.5 g L^{-1} (Δ).

P. tricornutum strains have already been isolated from low salinity waters (De Martino et al. 2007). At low salinity, this diatom changes its morphology mainly to oval

form, a stress morphology with accumulation of lipids. At normal seawater salinities the fusiform and the triradiate cells are predominant (De Martino et al. 2011).

Microscopic observations revealed that more than 99% of the cells exist in fusiform morphology, although in the culture grown at low salinities the cells seem to have less pigmentation. While at 20 g L^{-1} it is possible to see the cell with a brownish green lozenge. Under 2.5 and 5 g L^{-1} the culture has spheres of pigmentation distributed throughout the cell.

This spectrum of growth of this diatom is an advantage to control possible contamination on industrial scale. Furthermore, the growth at low salinity medium is important for industrial prevention of wear and tear of growth and biomass collection equipment's which is more exhausting at higher salinity.

After the study of growth, the growth rates for each one of the salinities and the biomass productivities were calculated, and the final values are shown in Table 1.

Table 1 - Volumetric productivity on biomass during whole test and the maximum in a short interval, and the growth rate on the exponential phase for each of the salinities in the study.

Salt (g L^{-1})	Maximum volumetric productivity (g L^{-1} day^{-1})	Volumetric productivity (g L^{-1} day^{-1})	Overall growth rate (day^{-1})
2.5	0.076 ± 0.008	0.050 ± 0.003	0.132 ± 0.008
5	0.077 ± 0.006	0.050 ± 0.002	0.126 ± 0.007
10	0.100 ± 0.016	0.058 ± 0.004	0.148 ± 0.012
20	0.086 ± 0.006	0.056 ± 0.003	0.131 ± 0.007

For the range of salinities tested there were not significant differences on mass productivity, such as, at maximum productivity the cultures have the same response ($p \geq 0.05$). Similarly, no significant differences were found for the growth rate ($p \geq 0.05$).

With these data, it is interesting to lower the salinity up to 2.5 g L^{-1} and achieve the same productivity in industrial scale, that could be a way to control some contaminants and less damage to production equipment promoted by exposure to high ionic forces (Thaulow & Sahu 2004).

As there are no growth differences between this range of salinities, the biochemistry constitution of the biomass produced under different salinities was analysed (Table 2).

Table 2 - Proximate composition of batch cultures grown in 5 L reactors using different salinities, results standardized so that salinity does not affect values (mean± standard deviation)

Salt (g L^{-1})	Proteins (%)	Lipids (%)	Carbohydrates (%)	Ashes (%)
2.5	53.6 ± 2.0	23.9 ± 2.7	22.4 ± 1.6	8.28 ± 0.19
5	54.6 ± 5.0	25.6 ± 2.2	19.7 ± 1.9	9.94 ± 0.88
10	54.7 ± 1.2	28.8 ± 1.1	18.6 ± 0.6	10.3 ± 0.2
20	51.2 ± 1.2	29.5 ± 0.4	19.3 ± 0.5	14.0 ± 0.1

The percentage of ashes in biomass and salt in culture medium have a correlation (r^2=0.96) with an intercept in origin of 7.86%, that is the percentage of micronutrients present in addition to sodium chloride.

The lipids amount of cultures grown in 20 g L^{-1} salt concentrations of was higher than for 2.5 g L^{-1} (p<0.05). However, no significant differences were obtained between intermediate concentrations of salt and each one of extreme salinity cultures.

All of culture conditions of salinity caused no significant differences in biomass protein composition ($p\geq0.05$).

To find if there was a difference between the intensifications of lipids composition under different salinities, the FAME profile was analysed, as shown in Table 3.

Previous analyses of FAME showed some differences between the minor constituents (García et al. 2000; Ryckebosch et al. 2014; Hamilton et al. 2015; Hamilton et al. 2016; Remmers & Martens 2017). Although some of FAME previous reported were not possible quantify, had been reported like hexadecadienoic (C16:2), hexadecatrienoic (C16:3) or hexadecatetraenoic (C16:4) acids (Reis et al. 1996; Remmers & Martens 2017).

Table 3 - Fatty acid methyl ester profile of batch cultures grown in 5 L reactors with different salinities. Values are given as means of total FAME percentage ± standard deviation (n = 3). n.d., not detected

FAME	% of total FAME			
	2.5 g L^{-1}	5 **g L^{-1}**	10 **g L^{-1}**	20 **g L^{-1}**
C14:0	3.2 ± 0.1	3.2 ± 0.1	3.7 ± 0.2	3.0 ± 0.1
C15:1	0.13 ± 0.01	0.11 ± 0.02	0.10 ± 0.02	0.11 ± 0.01
C15:0	0.24 ± 0.02	0.20 ± 0.01	0.20 ± 0.02	0.22 ± 0.03
C16:1	42 ± 1	40 ± 1	37 ± 1	39 ± 1
C16:0	7.7 ± 0.1	7.7 ± 0.2	7.1 ± 0.1	7.1 ± 0.1
C18:4 ω-3	1.1 ± 0.1	0.92 ± 0.02	1.0 ± 0.2	n.d.
C18:3 ω-6	0.52 ± 0.04	0.46 ± 0.07	0.55 ± 0.14	0.54 ± 0.01
C18:2 ω-6	2.2 ± 0.1	2.3 ± 0.1	2.6 ± 0.1	1.9 ± 0.1
C18:1	6.9 ± 0.1	7.6 ± 0.1	8.9 ± 0.1	9.4 ± 0.1
C18:0	0.19 ± 0.01	0.22 ± 0.01	0.44 ± 0.22	0.27 ± 0.01
C20:5 ω-3	26 ± 1	26 ± 1	28 ± 1	26 ± 1
C20:4 ω-6	n.d.	1.1 ± 1.1	n.d	n.d
C20:4 ω-3	0.41 ± 0.01	0.42 ± 0.01	0.46 ± 0.02	3.4 ± 0.1
C20:3	1.9 ± 0.1	1.9 ± 0.1	2.3 ± 0.1	3.9 ± 0.1
C20:2 ω-6	n.d.	n.d.	n.d.	0.38 ± 0.01
C20:1	0.69 ± 0.04	0.86 ± 0.08	0.60 ± 0.03	0.14 ± 0.01
C22:6 ω-3	3.9 ± 0.1	3.7 ± 0.2	3.7 ± 0.1	1.7 ± 0.2
C22:5 ω-3	0.81 ± 0.01	0.68 ± 0.04	0.84 ± 0.05	0.73 ± 0.01
C22:4 ω-3	n.d.	n.d.	0.11 ± 0.11	0.35 ± 0.01
C22:0	0.07 ± 0.07	n.d.	0.16 ± 0.03	n.d.
C24:1	0.19 ± 0.19	n.d.	0.70 ± 0.03	0.39 ± 0.04
C24:0	2.0 ± 0.1	2.0 ± 0.1	2.1 ± 0.1	1.8 ± 0.1
SFA	13 ± 1	13 ± 1	13 ± 1	12 ± 1
MUFA	50 ± 1	49 ± 1	47 ± 1	49 ± 1
PUFA	37 ± 1	38 ± 1	39 ± 1	39 ± 1
ω-3/ω-6	7.4 ± 0.2	5.9 ± 1.2	6.6 ± 0.2	5.4 ± 0.1
PUFA/SFA	2.8 ± 0.1	2.8 ± 0.1	2.8 ± 0.1	3.1 ± 0.1

The various salinities caused no differences when comparing the fraction of saturated fatty acids (SFA). In fact, differences were found for SFA, was an increase of tetradecanoate acid (C14:0) for biomass grown at salinity of 10 g L^{-1} ($p<0.05$).

Hexadecanoic acid (C16:0) is around of 7% of FAME, and it is the SFA with greatest percentage. Although, the results here obtained are lower than previously reported, it is always reported as the majority SFA (Siron et al. 1989; García et al. 2000; Hamilton et al. 2016). Other side, in accordance with other results that report 8% of the total FAME (Zhao et al. 2014).

Hexadecenoic acid (C16:1) is the FAME present in higher proportion like was previous reported (Hamilton et al. 2016), without differences between the culture condition of salinity as previous reported. This, monounsaturated FA (MUFA) is the sum of 9-hexadecenoic acid and the minor 7-hexadecenoic acid(Reis et al. 1996).

SDA was detected at the same level at the lowers salinities (2.5 to 10 g L^{-1}) approaching 1% of total FAME ($p \geq 0.05$). At the higher salinity it was not possible to quantify this omega 3 PUFA, in this study.

EPA was produced at the same level at all salinities about 26% of total FAME, with a soft increase on the 10 g L^{-1}, this is the higher omega 3 produced by *P. tricornutum* (Zhao et al. 2014). The fatty acids of the EPA synthesis pathway: eicosatetraenoate (C20:4 ω-3) and eicosatrienoate acid (C20:3 ω-3) are significantly increased in the biomass produced at 20 g L^{-1}. The chromatographic method does not have the resolution to elute the two isomers of C20:3 of the in different peaks (the two isomers are present in the commercial standard solution and was being eluted at the same pick of chromatogram), being the result presented by the sum of both omega 6 and 3 isomers.

DHA was detected at higher extent in the biomass produced in less salinity concentration. The others omega 3 with 22 carbons chain length but fewer double bonds were present in similar contents ($p<0.05$).

Although, even cultures grown at 20 g L^{-1} have a higher percentage of total lipids, this biomass has less DHA with more than 0.6 g 100 g^{-1} than the others biomass grown

at 10, 5 and 2.5 g L^{-1} that were found to have more than 1.3 g 100 g^{-1} (p<0.05). EPA was found to have the same level for all for all salinities under which the biomass was grown, with more than 9 g 100 g^{-1} (p≥0.05). The quantification of FA per biomass was done without an inner standard that do not allow the determination of the error associated to recovery coefficient of all the extraction process and from chromatograph.

3.2 Growth and photosynthetic efficiency on large scale photobioreactor

After understanding the growth of *P. tricornutum* in different salinities at the laboratory scale, we advanced to the large outdoor scale PBR. After growing them in GWP the problems came when the cultures were scaled-up to 2500 L tubular PBR, with a very difficult task of maintaining the temperature of the PBR below 28ºC. The thermoregulation in this system reached its the maximum of response and was unable to decrease the temperature on very hot days of spring-summer.

The combination of this thermal stress and the lowering of salinity in the culture had as result the death of the culture in the PBR in the second day of growth, similar to previous reports (Stickney 1964; Lylis & Trainor 1973), or a drastic change of morphology that lacked the industrial and commercial value. When growing *P. tricornutum* in tubular PBR and, subjecting the culture to high temperature (more than 28ºC) for a time longer than 4 hours per day at 10 g L^{-1} it resulted in increasing levels of round and oval morphologies on culture of more than 70%. As previous reported (De Martino et al. 2011) a higher risk of biofilm occurs, hampering biomass collection.

The geometry of reactor in which it was possible to have more density of culture was the GWP (p<0.05), as shown in Figure 10. It was possible to have the same density in 35000 L PBR with lowers initial densities than in the 10000 L PBR after eight days of growth (Figure f B and g B).

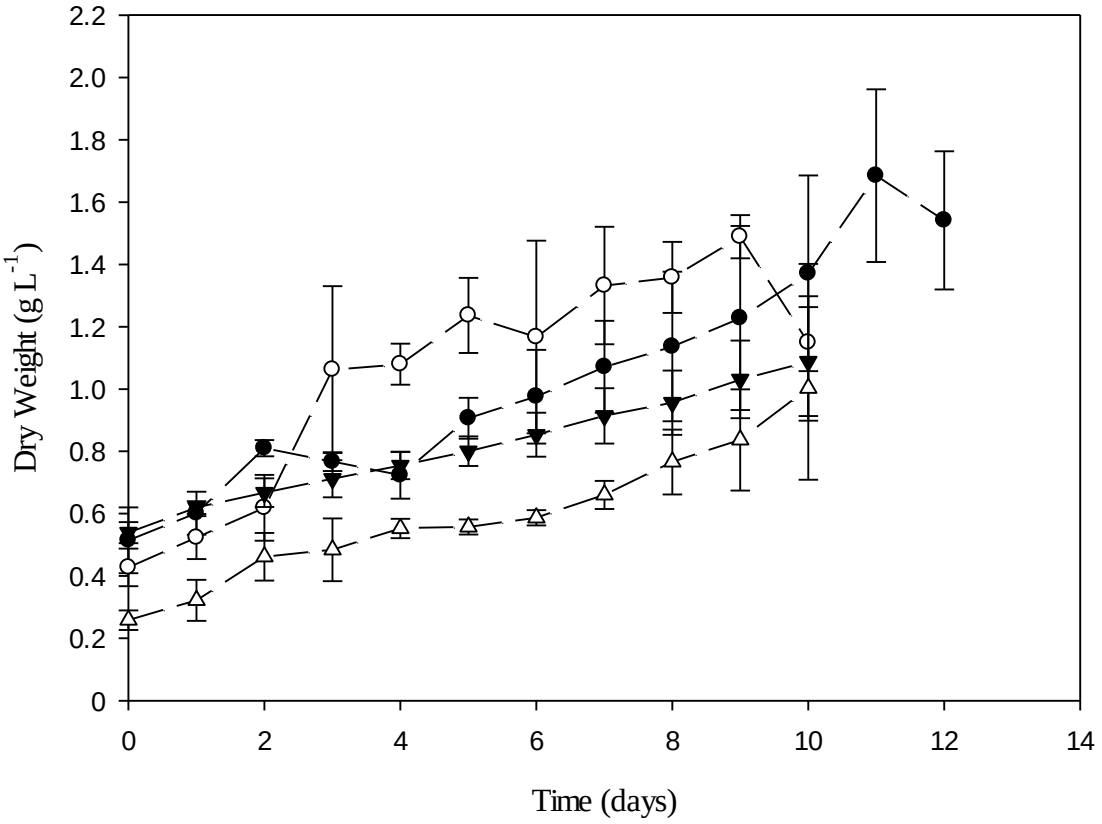

Figure 10 - Batch growth of *P. tricornutum* in different geometries of reactor. Dry weight of culture at 125 L GWP(●); at 2500 Tubular PBR (○); at 10000 Tubular PBR (▼) and at 35000 Tubular PBR (Δ)

After the preliminary studies, the growth assay in the different reactors was done at 20 g L^{-1} and the volumetric and areal productivities, are shown in Table 4.

Table 4 – Maximum volumetric productivity, global volumetric productivity, maximum areal productivity and global areal productivity for the different geometries of outdoor PBR where growth was analysed. Values are given as means ± standard deviation (n = 3).

Reactor geometry	**Maximum volumetric productivity (g L^{-1} day^{-1})**	**Volumetric productivity (g L^{-1} day^{-1})**	**Maximum areal productivity (g m^{-2} day^{-1})**	**Areal productivity (g m^{-2} day^{-1})**
GWP 125 L	0.146 ± 0.010	0.080 ± 0.007	18.9 ± 1.3	9.97 ± 0.94
PBR 2500 L	0.235 ± 0.043	0.123 ± 0.009	12.8 ± 1.0	6.17 ± 0.43
PBR 10000 L	0.140 ± 0.007	0.070 ± 0.005	45.0 ± 2.3	22.5 ± 1.6
PBR 35000 L	0.175 ± 0.017	0.069 ± 0.008	48.5 ± 4.8	19.1 ± 2.1

The system with the highest volumetric productivity was the 2500 L PBR, with a statistically significant difference from the other reactors (p<0.05), reaching the maximum value of 0.235 g L^{-1} day^{-1} and with a global volumetric productivity of 0.123 g

L^{-1} day^{-1}. Even though it is lower than 1.4 g L^{-1} day^{-1} previously reported for a helical tubular PBR (Fernández et al. 2003), we have to take into account that the differences of geometry and culture medium have a strong influence on biomass productivity. However, when analysing the areal productivity, 2500 L PBR was the one with lower productivity, followed by the GWP with 125 L. The most productive were the industrial PBR of 10000 L and 35000 L without any significant differences between them ($p \geq 0.05$). The areal productivity was 12.8 g m^{-2} day^{-1} in a 2500 L PBR, 18.9 g m^{-2} day^{-1} in the GWP and 45.0 and 48.5 g m^{-2} day^{-1} in 10000 L and 35000 L PBR, respectively ($p<0.05$). These values are better than 11.4 g m^{-2} day^{-1} reported for a PBR (Benavides et al. 2013) and better than 21.0 g m^{-2} day^{-1} reported for an indoor annular 250 L PBR (Buono et al. 2016). Still, the maximum areal productivity of the GWP and 2500 L PBR had the same productivities ($p \geq 0.05$), however, less than the industrial reactors.

Table 5 shows the growth rates and the photosynthetic efficiencies of *P. tricornutum* in the different reactors.

Table 5 – *P. tricornutum* growth rate and photosynthetic efficiency in the different reactors.

Reactor geometry	**Growth rate (day^{-1})**	**Photosynthetic efficiency (%)**
GWP 125 L	0,107 ± 0,003	1.01 ± 0.46
PBR 2500 L	0,190 ± 0,013	1.27 ± 0.63
PBR 10000 L	0,116 ± 0,006	2.08 ± 0.78
PBR 35000 L	0,141 ± 0,017	2.21 ± 0.82

The growth of *P. tricornutum* culture was faster in both 2500 L and 35000 L PBR's, with specific growth rate of 0.19 day^{-1} and 0.14 day^{-1}, respectively, without statistic significant differences between each two ($p \geq 0.05$). On the other hand, the GWP and 10000 L PBR allowed slower growth rates with 0.11 and 0.12 day^{-1} respectively ($p<0.05$).

The photosynthetic efficiency was identical in the 125 L GWP and 2500 L tubular PBR, with an efficiency of 1.01% and 1.27%, respectively. More efficiency was seen in the industrial reactors, with 2.08% in a 10000 L and 2.21% in a 35000 L PBR, without differences between industrial reactors efficiencies (p<0.05).

A larger volume in the same area became the industrial an interesting efficiency juxtaposition to GWP or a pilot scale PBR, the increase of photic region with an expansion of height of this section of the reactor. Although a soft reduction of height of industrial reactors could improve the volumetric productivity with the aim of not losing areal productivity and photosynthetic efficiency. If the geometry of the reactor make it possible, it would became to a higher concentration with the intention of minimize the downstream process and the recourses needed to produce the same quantity of biomass.

3.3 Biochemistry of biomass grown in industrial reactors

In large scale reactor, the differences at biochemical level between the two states of culture were studied (Table 6). The entitled benthic culture was a biomass that had more than 70% of cells in clusters (observation does not show, with a higher percentage of cluster and round cells than Figure b C in appendix), and the tubular PBR inner surface was a dense biofilm. The planktonic culture had more than 99% of cells in fusiform morphology and some cells in triradiate (Figure b A in appendix).

Table 6 - Proximate composition of batch cultures grown in large scale reactors in different states of morphology, results standardized so that salinity does not affect macromolecules values (mean± standard deviation)

Culture	Proteins (%)	Lipids (%)	Carbohydrates (%)	Ashes (%)
Benthic	44.1 ± 0.8	14.7 ± 0.4	41.2 ± 0.7	11.4 ± 0.
Planktonic	52.8 ± 1.5	22.2 ± 0.6	25.0 ± 0.7	13.2 ± 0.4
Industrial	53.1 ± 7.4	27.2 ± 4.0	19.7 ± 2.8	17.0 ± 2.4

The industrial biomass biochemistry of culture was similar to biomass growth in the airlift at lab scale, with a salinity of 20 g L^{-1} (p≥0.05). The industrial culture of *P.*

tricornutum was a sample of the 35000 L PBR at the end of exponential growing phase, and the difference of geometry of reactor does not change the macromolecule distribution. This suggests that the quality of biomass is similar after the scale-up, an important fact that customers require in the industry of microalgae.

Comparing the benthic and planktonic, these two cultures were very different in terms of biochemical macromolecules. The percentage of protein decreases in benthic morphology, as do the lipids, with a consequential increase in carbohydrates.

When *P. tricornutum*, like other diatom, senses stress conditions, it changes into benthic morphology, that is a form that allow the algae to reduce overkill radiation, promote cell attachment and adapt to nutrient limitation; in this stage the cluster of cells is linked by polysaccharides structed (Abdullahi et al. 2006; Willis et al. 2013), so the increase of carbohydrates is predictable.

The main extracellular polysaccharides are mannose, glucose, galactose xylose and rhamnose, in sequential predominant monomer (Abdullahi et al. 2006). The stage of oval morphology in biofilm increases fucose and rhamnose, which could be related with adhesion properties, because these monomers are hydrophobic enhancing the molecular interactions between the polymers (Willis et al. 2013).

To know more specifically the changes on lipids, it was studied the FAME profile (Table 7).

Between the two morphologies differences at levels of as the relative percentage of FAME were noted, although no differences between the percentage of SFA, MUFA and PUFA on two morphologies were found. The frustule morphology has an increase of tetradecanoate and pentadecenoic acids, although both pentadecanoic and hexadecanoic acids increased in the biofilm *P. tricornutum* ($p<0.05$), whereas hexadecenoic acid proportions displayed no difference ($p\geq0.05$).

Table 7 - Fatty acid profile of batch in large scale with different morphologies. Values are given as means of total FAME percentage ± standard deviation (n = 3). n.d., not detected

FAME	% of total FAME	
	Benthic	**Planktonic**
C14:0	3.1 ± 0.1	4.1 ± 0.1
C15:1	n.d.	0.11 ± 0.02
C15:0	0.29 ± 0.01	0.18 ± 0.01
C16:1	25 ± 1	24 ± 1
C16:0	7.5 ± 0.1	4.9 ± 0.1
C18:4 ω-3	1.2 ± 0.1	n.d.
C18:3 ω-6	0.95 ± 0.03	0.20 ± 0.01
C18:2 ω-6	2.9 ± 0.1	2.7 ± 0.1
C18:1	21 ± 1	8.0 ± 0.1
C18:0	0.49 ± 0.01	0.20 ± 0.01
C20:5 ω-3	17 ± 1	23 ± 1
C20:4 ω-6	2.4 ± 0.3	0.9 ± 0.9
C20:4 ω-3	0.79 ± 0.02	2.5 ± 0.1
C20:3	0.78 ± 0.09	5.5 ± 0.1
C20:2 ω-6	n.d.	1.7 ± 0.1
C20:1	n.d.	0.08 ± 0.01
C22:6 ω-3	2.7 ± 0.1	2.0 ± 0.2
C22:5 ω-3	0.90 ± 0.45	0.99 ± 0.08
C22:4 ω-3	n.d.	0.39 ± 0.03
C22:0	0.61 ± 0.05	n.d.
C24:1	n.d.	0.85 ± 0.09
C24:0	1.7 ± 0.1	1.9 ± 0.1
SFA	14 ± 1	14 ± 1
MUFA	46 ± 1	40 ± 4
PUFA	40 ± 1	47 ± 7
ω-3/ω-6	1.5 ± 0.1	3.2 ± 0.7
PUFA/SFA	2.9 ± 0.1	3.5 ± 0.6

The FAME with eighteen carbons increase in the biofilm except the LA that has no differences in portion between the two stages. SDA is present at near 1% like what was quantified in the low salinities assays.

EPA was produced at the same level at the two morphologies, in this study about 23% of FAME in fusiform ($p \geq 0.05$). The omega 3 PUFA included in EPA synthesis pathway are increased in fusiform cells, although eicosatetraenoate acid omega 6 is increased in biofilm ($p < 0.05$).

The FAME with twenty-two carbons are similar in both morphologies, as well as DHA and DPA. However, the docosatetraenoic acid are not detected in benthic and docosanoic acid are increased.

Even with the highest percentage of lipids in fusiform culture, this biomass has the same DHA and EPA that is present in benthic culture, with 0.9 and 10 g 100 g^{-1} of biomass, respectively ($p \geq 0.05$).

In the same way, culture of *P. tricornutum* in frustule morphology at large scale does not have differences to a culture in 5 L reactor at salinity of 20 g L^{-1} in the profile of fatty acids.

Nevertheless, carbohydrates are increased in benthic culture of *P. tricornutum* and, that culture has the same percentage of fatty acid which improves the price per kilogram of biomass, like EPA and DHA (Leu & Boussiba 2014). Therefore, if it was possible to harvest the culture from the reactor, these should have the same interest to microalgae market, but this biomass increases the production cost with fewer productivities and harvesting efficiencies.

3.4 Stoichiometric equation for *P. tricornutum* and CO_2 sequestering efficiency

The stoichiometric of *P. tricornutum* grown in 10000 L industrial reactors was determined: $CH_{1.9}N_{0.14}O_{0.42}$, as reported for general microalgae (Myint et al. 2013). Knowing by CHN analyse of biomass that 53% (m/m) is carbon, 8% (m/m) is hydrogen and 8% (m/m) is nitrogen in base without ash, the remain was considered oxygen.

Analysis of mass balance for each element provided the following stoichiometric equation for *P. tricornutum* grown in 10000 L PBR:

$$CO_2 + 0.12NO_3^{2-} + 0.83H_2O + 0.24H^+ \xrightarrow{\text{light}} 0.87CH_{1.9}N_{0.14}O_{0.42} + 1.3O_2 + 0.022C_6H_{12}O_6 \quad (13)$$

In the 10000 L PBR the CO_2 sequestration by biomass formation was 0.87 moles of biomass per mole of CO_2. That resulted in the mitigation of 2.3 gram CO_2 per of biomass formed, that is more 1.6-2 g g^{-1} than predicted in past reports (Sayre 2010).

The stoichiometry of *P. tricornutum* growth in 35000 L PBR was determined: $CH_{1.9}N_{0.14}O_{0.40}$, knowing by CHN analysis of biomass that 54% (m/m) is carbon, 8% (m/m) is hydrogen and 9% (m/m) is nitrogen in base without ash.

Then, mass balance analysis of each element provided this stoichiometric equation for *P. tricornutum* grown in 35000 L PBR:

$$CO_2 + 0.11NO_3^{2-} + 0.83H_2O + 0.22H^+ \rightarrow 0.81CH_{1.9}N_{0.14}O_{0.42} + 1.3O_2 + 0.031C_6H_{12}O_6 \quad (14)$$

For it side, in a 35000 L PBR the CO_2 sequestration by biomass formation is 0.81 moles of biomass per mole of CO_2. That result in a mitigation of 2.5 g g^{-1}, that is better than a 10000 L reactor.

To improve the sequestration of CO_2 by the extracellular products biomass of *P. tricornutum*, its production pathway must be favoured. However, by improving the production of extracellular products and only harvesting the biomass we are losing potential value products.

Finally, after the stoichiometric analysis, CO_2 consumption was determined. Moreover, the efficiency of CO_2 mitigation of *P. tricornutum* in industrial reactors was studied.

For this analysis, all inputs and outputs of carbon from PBR were quantified and analysed, as shown in Figure 11.

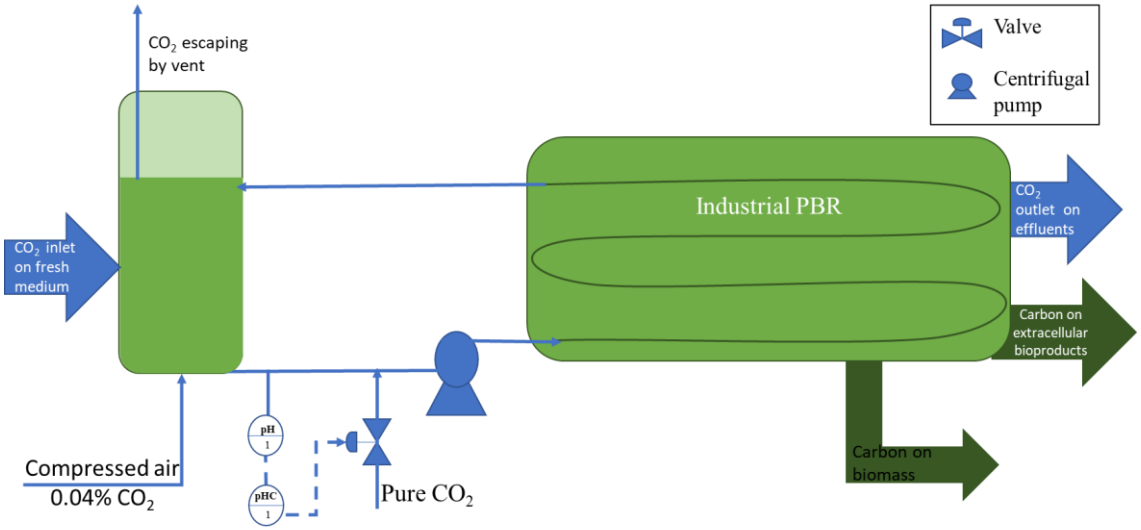

Figure 11 - Diagram of industrial PBR (10000 L or 35000 L) with demonstrations of carbon inputs and outputs. pH is a sensor of pH, pHC is the controller that responds to changes of pH; solid line represents pipe and dashed line means an electric signal conduction. Full blue arrow is CO_2 in medium, full green arrow with black letters is carbon left in the form of biomass and with white letters is carbon left in form of extracellular bioproducts.

The temperature, salinity and the pH of culture medium were similar in the first day and at the end of biomass growth. Assuring this, the percentage of CO_2 dissolved remains the same (Weiss 1974; Laws et al. 1997; Hill et al. 2014); this removes two variables to study this system.

The CO_2 injected by air bubbling in the pond and the pure CO_2 used to lower the pH of medium was quantified. Therefore, the biomass and its percentage of carbon as well as the amount of extracellular organic carbon was quantified. The CO_2 that leaves the PBR is the remaining CO_2 that was injected in the reactor.

The result in the efficiency of sequestering of CO_2 is shown in Table 8. In a 10000 L PBR, the CO_2 sequestration efficiency was 60%. However, in the large PBR the efficiency decreased to 41%.

The efficiency in sequestering CO_2 in 10000 L PBR was similar to what was previously reported for *P. tricornutum* in a 50 L tubular airlift PBR, that has a maximum of 63% in daylight conditions (Sobczuk et al. 2000).

Table 8- Efficiency of sequestering by *P. tricornutum* in industrial PBR.

Reactor	% of CO2 sequestered
1st assay in 10000 L reactor	57.9
2nd assay in 10000 L reactor	66.8
3rd assay in 10000 L reactor	55.2
Average of 10000 L reactor	60 ± 5
1st assay in 35000 L reactor	42.8
2nd assay in 35000 L reactor	38.8
Average of 35000 L reactor	41 ± 2

A second assay in the 10000 L PBR was undertaken at the same time as the first assay in the 35000 L one, as were the third assay for 10000 L and second one for 35000 L. The decrease of efficiency between assays keep up with the photosynthetic efficiency which indicates a decrease in efficiency of solar energy use resulting in greater losses of CO_2 by vent.

The 35000 L has a photic zone twice as longer as the 10000 L reactor, which leads to a longer circulation time in photic zone of gas and biomass which could increase uptake of CO_2.

To increase the usage efficiency of CO_2 injected in the reactor, the control of CO_2 injection to this species could be optimized. The 35000 L tubular PBR has an impulse of this gas longer than in the 10000 L, so a possible efficiency improvement could be the reduction of this time.

At the same time, the mixture of biomass and gas, and consequently the contact of these two components, is lower in the 35000 L reactor. Along the path of the photic zone the culture has characteristic problems of a plug-flow reactor. On the photic zone the pH rises and the oxygen produced by the cells accumulates in the medium, but the major limitation to growth is the concentration of CO_2 dissolved in the medium, which is lower than that consumed by the microalgae (Dragone et al. 2010; Kumar et al. 2011).

Since the K_La (volumetric CO_2 transfer coefficient) is lower it is difficult to provide all the CO_2 the cells need to improve their growth. The small air bubbles coming out of the diffuser exchange CO_2 with cells, but the weak dissolution in the medium provides a separation of gas phase and culture medium with the microalgae, resulting in a system with high limitations to the mass transfer of the carbon source (Sobczuk et al. 2000; Kumar et al. 2011).

The solution to improve the fixation efficiency could be the place diffusers along the photic zone or increase the moisture with a turbulent regime inside the tubes, with disturbances on the flow or increasing the flow velocity.

4 Conclusions and future work

P. tricornutum have a cellular metabolism that allows the growth in salinities ranging between 2.5 and 20 g L^{-1}, without significant differences in growth. The decrease of salt concentration in the culture medium reduces the percentage of lipids at 2.5 g L^{-1} when compared to cultures grown at 20 g L^{-1}. Although, the percentage of EPA is similar under all salinities understudy, lower salinities (2.5, 5 and 10 g L^{-1}) increase the percentage of DHA and SDA in the FAME profile.

The 2500 L tubular PBR displayed higher volumetric productivities compared to the 35000 L industrial tubular PBR. However, both 10000 L and 35000 L PBR showed higher areal productivities and photosynthetic efficiencies, due to the higher volume of culture per area of land.

In large scale reactors, the benthic and planktonic stages of *P. tricornutum* were studied. Although the benthonic phase has an increase of carbohydrates and significant differences in lipid profile, the DHA and EPA are present in similar levels in both stages.

The growth of *P. tricornutum* has a mitigation of 2.4 g of CO_2 per g of biomass produced. In addition, the CO_2 fixation efficiency registered was 60% in 10000 L PBR and 41% on 35000 L PBR. This decrease of efficiency was probably related with problems of scale-up, where the mixture of culture medium and gas is a determining factor.

In the future, a multivariate analysis of the growth parameters (e.g. temperature, radiation and nutrients concentration) used throughout this study might highlight important information on ways to improve the growth performance of *P. tricornutum*.

In order to improve the fixation of CO_2, further studies on the influence of different pH set points in the CO_2 should be carried out, as this parameter has major consequences on growth. A similar study in autumn or spring, when it is easier to control

the temperature and avoid cellular stress, should also be done to compare the results, such as the growth performance and the impact on biomass biochemistry. Future studies on this strain should also focus their efforts on the determination of fucoxanthin, as this is a high value metabolite and a current trend in microalgal biotechnology.

Finally, it is important to improve the harvesting costs of this strain. Therefore, further studies on the sedimentation or natural flocculation of this strain can effectively reduce the current costs of the whole microalgae production process.

5 Bibliographic references

Abdullahi, A.S., Underwood, G.J.C. and Gretz, M.R., 2006. Extracellular matrix assembly in Diatoms (Bacillariophyceae). V. environmental effects on polysaccharide synthesis in the model Diatom, *Phaeodactylum tricornutum. Journal of Phycology*, 42, pp.363–378.

Benavides, A.M.S., Torzillo, G., Kopecký, J. and Masojídek, J., 2013. Productivity and biochemical composition of *Phaeodactylum tricornutum* (Bacillariophyceae) cultures grown outdoors in tubular photobioreactors and open ponds. *Biomass and Bioenergy*, 54, pp.115–122.

Bhola, V., Swalaha, F., Kumar, R.R., Singh, M. and Bux, F., 2013. Overview of the potential of microalgae for CO_2 sequestration. *International Journal of Environmental Science and Technology*, 11, pp.2103-2118.

Bligh, E.G. and Dyer, W.J., 1959. A rapid method of total lipid extraction and purification. *Canadian Journal of Biochemistry and Physiology*, 37, pp.911-917.

Buono, S., Colucci, A., Angelini, A., Langellotti, A.L., Massa, M., Martello, A., Fogliano, V. and Dibenedetto, A., 2016. Productivity and biochemical composition of *Tetradesmus obliquus* and *Phaeodactylum tricornutum*: effects of different cultivation approaches. *Journal of Applied Phycology*, 28, pp.3179–3192.

Callejón-Ferre, A.J., Velázquez-Martí, B., López-Martínez, J.A. and Manzano-Aguhliaro, F., 2011. Greenhouse crop residues: Energy potential and models for the prediction of their higher heating value. *Renewable and Sustainable Energy Reviews*, 15, pp.948–955.

Cerón-García, M.C., Fernandez-Sevilla, J.M., Acién-Fernández, F.G., Molina-Grima, E. and Camacho, F.G., 2000. Mixotrophic growth of *Phaeodactylum tricornutum* on glycerol: growth rate and fatty acid profile. *Journal of Applied Phycology*, 12, pp.239–248.

Cerón-García, M.C., Camacho, F.G., Mirón, A.S., Fernandez-Sevilla,J.M., Chisti, Y. and Molina-Grima,E., 2006. Mixotrophic production of marine microalga *Phaeodactylum tricornutum* on various carbon sources. *Journal of microbiology and biotechnology*, 16, pp.689–694.

De Martino, A., Meichenin, A., Shi, J., Pan, K.H. and Bowler, C., 2007. Genetic and phenotypic characterization of *Phaeodactylum tricornutum* (Bacillariophyceae) accessions. *Journal of Phycology*,43, pp.992-1009.

De Martino, A., Bartual, A.,Willis, A., Meichenin, A., Villazán, B., Maheswari, U. and Bowler, C., 2011. Physiological and molecular evidence that environmental changes elicit morphological interconversion in the model diatom *Phaeodactylum tricornutum*. *Protist*, 162, pp.462–481.

Desbois, A.P., Mearns-spragg, A. and Smith, V.J., 2009. A fatty acid from the Diatom *Phaeodactylum tricornutum* is antibacterial against diverse bacteria including

multi-resistant *Staphylococcus aureus* (MRSA). *Marine Biotechnology*, 11 pp.45–52.

Dragone, G., Fernandes, A., Vicente, A.A. and Teixeira, J.A., 2010. Third generation biofuels from microalgae. in *Current research, technology and education topics in applied microbiology and microbial biotechnology*. pp. 1355–1366.

Fernández, F.G.A., Hall, D.O., Guerrero, E.C., Rao, K.K. and Grima, E.M., 2003. Outdoor production of *Phaeodactylum tricornutum* biomass in a helical reactor. *Journal of Biotechnology*, 103, pp.137–152.

Fonseca, D.B., Guerra, L.T., Santos, E.T., Mendonça, S.H., Silva, J.G., Costa, L.A. and Navalho, J.C., 2016. ALGAFARM: A case study of industrial *Chlorella* production. in *Microalgal production for biomass and high-value products*. pp. 295–310.

Granum, E., Kirkvold, S. and Myklestad, S.M., 2002. Cellular and extracellular production of carbohydrates and amino acids by the marine diatom *Skeletonema costatum*: diel variations and effects of N depletion. *Marine Ecology Progress Series*, 242, pp.83–94.

Gügi, B., Costaouec, T.L., Burel, C., Lerouge, P., Helbert, W., Bardor, M., 2015. Diatom-specific oligosaccharide and polysaccharide structures help to unravel biosynthetic capabilities in Diatoms. *Marine Drugs*, 13, pp.5993–6018.

Hamilton, M.L., Haslam, R.P., Napier, J.A. and Sayanova, O., 2014. Metabolic engineering of *Phaeodactylum tricornutum* for the enhanced accumulation of omega-3 long chain polyunsaturated fatty acids. *Metabolic Engineering*, 22, pp.3–9.

Hamilton, M.L. Warwick, J., Terry, A., Allen, M.J., Napier, J.A. and Sayanova, O., 2015. Towards the industrial production of omega- 3 long chain polyunsaturated fatty acids from a genetically modified Diatom *Phaeodactylum tricornutum*. *PLoS ONE*, 10, pp.1–15.

Hamilton, M.L., Powers, S., Napier, J.A. and Sayanova, O, 2016. Heterotrophic production of omega-3 long-chain polyunsaturated fatty acids by trophically converted marina Diatom *Phaeodactylum tricornutum*. *Marine Drugs*, 14, article no 53

Hildebrand, M., Davis, A.K., Smith, S.R., Traller, J.C. and Abbriano, A., 2012. The place of diatoms in the biofuels industry. *Biofuels*, 3, pp.221–240.

Hill, P.S., Tripati, A.K. and Schauble, E.A., 2014. Theoretical constraints on the effects of pH, salinity, and temperature on clumped isotope signatures of dissolved inorganic carbon species and precipitating carbonate minerals. *Geochimica et Cosmochimica Acta*, 125, pp.610–652.

Hualian, W., Tao, L., Guanghua, W., Shikun, D., Hui, H. and Wenzhou, X., 2015. A comparative analysis of fatty acid composition and fucoxanthin content in six *Phaeodactylum tricornutum* strains from different origins *. *Chinese Journal of Oceanology and Limnology*, 34, pp.391-398.

Jaubert, M., Bouly, J.P., d'Alcalà, M.R. and Falciatore, A., 2017. Light sensing and responses in marine microalgae. *ScienceDirect*, 37, pp.70-77.

Johansen, J.R., 1991. Morphological variability and cell wall composition of *Phaeodactylum tricornutum* (Bacillariophyceae), *Great Basin Naturalist*, 51, pp.310-315.

Khozin-goldberg, I., Iskandarov, U. and Cohen, Z., 2011. LC-PUFA from photosynthetic microalgae: occurrence, biosynthesis, and prospects in biotechnology. *Applied Microbiology Biotechnology*, 91, pp.905–915.

Kosakowska, A., Lewandowska, J., Ston, J. and Burkiewicz, K., 2004. Qualitative and quantitative composition of pigments in *Phaeodactylum tricornutum* (Bacillariophyceae) stressed by iron. *BioMetals*, 17, pp.45–52.

Kumar, K., Dasgupta, C.N., Nayak, B., Lindblad, P. and Das, D., 2011. Development of suitable photobioreactors for CO_2 sequestration addressing global warming using green algae and cyanobacteria. *Bioresource Technology*, 102, pp.4945–4953.

Kwak, H.W., Kang, M.J., Bae, J.H., Hur, S.S., Kim, I.S., Park,Y.H. and Lee, K.H., 2014. Fabrication of *Phaeodactylum tricornutum* extract-loaded gelatin nanofibrous mats exhibiting antimicrobial activity. *International Journal of Biological Macromolecules*, 63, pp.198–204.

Laws, E.A., Bidigare, R.R. and Popp, B.N., 1997. Effect of growth rate and CO_2 concentration on carbon isotopic fractionation by the marine diatom *Phaeodactylum tricornutum*. Limnology and Oceanography, 42, pp.1552–1560.

Lepage, G. and Roy, C.C., 1984. Improved recovery of fatty acid through direct transesterification without prior extraction or purification. *Journal of Lipid Research*, 25, pp.1391-1396

Leu, S. and Boussiba, S., 2014. Advances in the Production of High-Value Products by Microalgae. *Industrial Biotechnology*, 10, pp.169–183.

Lewin, J.C., Lewin, R.A. and Philpott, D.E., 1958. Observations on *Phaeodactylum tricornutum*. *Journal of General Microbiology*, 18, pp.418-426.

Liang, Y., Sun, M., Tian, C., Cao, C. and Li, Z., 2014. Effects of salinity stress on the growth and chlorophyll fluorescence of *Phaeodactylum tricornutum* and *Chaetoceros gracilis* (Bacillariophyceae). *Botanica Marina*, 57, pp.469–476.

Liu, X., Duan, S., Li, A., Xu, A., Cai, Z. and Hu, Z., 2009. Effects of organic carbon sources on growth, photosynthesis, and respiration of *Phaeodactylum tricornutum*. *Journal of Applied Phycology*, 21, pp.239–246.

Longworth, J., Wu, D., Huete-Ortega, M., Wright, P.C. and Vaidyanathan, S., 2016. Proteome response of *Phaeodactylum tricornutum*, during lipid accumulation induced by nitrogen depletion. *Alga Research*, 18, pp.213–224.

Lylis, J.C. and Trainor, F.R., 1973. The heterotrophic capabilities of *Cyclotella meneghiniana*. *Journal of Phycology*, 9, pp.365–369.

Malm, A. & Hornborg, A., 2014. The geology of mankind? A critique of the Anthropocene narrative. *The Anthropocene Review*, 1, pp.62-69.

Marinho, Y.F., Brito, L.O., Campos, C.V.F.S., Severi, W., Andrade, H.A. and Galvez, A.O., 2017. Effect of the addition of *Chaetoceros calcitrans, Navicula sp. and Phaeodactylum tricornutum* (diatoms) on phytoplankton composition and growth of *Litopenaeus vannamei* (Boone) postlarvae reared in a biofloc system. *Aquaculture Research*, 48, pp.4155-4164

Martins, S.I.G., 2017. Impacts of CO_2 induced ocean acidification on predator detection ability and development of temperature fish. MSc. thesis, *Instituto Universitário de Ciências Psicológicas, Sociais e da Vida*, 51p.

Mata, T.M., Melo, A.C., Simões, M. and Caetano, N.S., 2012. Parametric study of a brewery effluent treatment by microalgae *Scenedesmus obliquus*. *Bioresource Technology*, 107, pp.151–158.

Mikami, K. and Hosokawa, M., 2013. Biosynthetic pathway and health benefits of fucoxanthin, an algae-specific xanthophyll in brown seaweeds. *International Journal of Molecular Sciences*, 14, pp.13763–13781.

Morais, K.C.C., Ribeiro, R.L.L., Santos, K.R., Taher, D.M., Mariano, A.B. and Vargas, J.V.C., 2009. *Phaeodactylum tricornutum* microalgae growth rate in heterotrophic and mixotrophic conditions, *Engenharia Térmica* 8, pp.84–89.

Mühlroth, A., Li, K., Røkke, G., Winge, P., Olsen, Y., Hohmann-Marriott, M. F., Vadstein, O. and Bones, A.M., 2013. Pathways of lipid metabolism in marine algae, co-expression network, bottlenecks and candidate genes for enhanced production of EPA and DHA in species of Chromista. *Marine drugs*, 11, 4662-4697.

Mutanda, T., Ramesh, D., Karthikeyan, S., Kumari, S., Anandraj, A. and Bux, F., 2011. Bioprospecting for hyper-lipid producing microalgal strains for sustainable biofuel production. *Bioresource Technology*, 102, pp.57–70.

Myint, M.T., Ghassemi, A. and Nirmalakhandan, N., 2013. A generic stoichiometric equation for microalgae – microorganism nexus by using clarified domestic wastewater as growth medium. *Desalination and Water Treatment*, 51, pp.6632–6640.

Niu, Y.F., Wang, X., Hu, D.X., Balamurugan, S., Li, D.W., Yang, W.D., Liu, J.S. and Li, H.Y., 2016. Molecular characterization of a glycerol-3-phosphate acyltransferase reveals key features essential for triacylglycerol production in *Phaeodactylum tricornutum*. *Biotechnology for Biofuels*, 9, article no.60.

Nunez, M. and Quigg, A., 2016. Changes in growth and composition of the marine microalgae *Phaeodactylum tricornutum* and *Nannochloropsis salina* in response to changing sodium bicarbonate concentrations. *Journal of Applied Phycology*, 28, pp.2123-2138.

Pereira, H., Barreira, L., Figueiredo, F., Custódio, L., Vizetto-Duarte, C., Polo, C., Rešek, E., Engelen, A. and Varela, J., 2012. Polyunsaturated fatty acids of marine

macroalgae: potential for nutritional and pharmaceutical applications. *Marine drugs*, 10, pp.1920–1935.

Pereira, H., Gangadhar, K.N., Schulze, P.S.C., Santos, T., De Sousa, C.B., Schueler, L. M., Custódio, L., Malcata, F.X., Gouveia, L., Varela, J.C.S. and Barreira, L, 2016. Isolation of a euryhaline microalgal strain, *Tetraselmis* sp. CTP4, as a robust feedstock for biodiesel production. *Scientific Reports*, 6, article no.35663.

Pérez, E. B., Pina, I. C. and Rodríguez, L.P., 2008. Kinetic model for growth of *Phaeodactylum tricornutum* in intensive culture photobioreactor. Biochemical Engineering Journal, 40, pp.520–525.

Pires, J. C. M., Alvim-Ferraz, M. C. M., Martins, F. G. and Simões, M., 2012. Carbon dioxide capture from flue gases using microalgae: Engineering aspects and biorefinery concept. *Renewable and Sustainable Energy Reviews*, 16, pp.3043–3053.

Prestegard, S.K., Erga, S.R., Steinrücken, P., Mjøs, S.A., Knutsen, G. and Rohloff, J., 2015. Specific metabolites in a *Phaeodactylum tricornutum* strain isolated from Western Norwegian Fjord Water. *Marine drugs*, 14, article no.9.

Prestegard, S.K., Knutsen, G. and Herfindal, L., 2014. Adenosine content and growth in the diatom *Phaeodactylum tricornutum* (Bacillariophyceae): Effect of salinity, light, temperature and nitrate. *Diatom research*, 29, pp.361-369.

Raposo, M.F.D.J., de Morais, A.M.M.B. and de Morais, R.M.S.C., 2015. Carotenoids from marine microalgae: A valuable natural source for the prevention of chronic diseases. *Marine drugs*, 13, pp.5128-5155.

Reis, A., Gouveia, L., Veloso, V., Fernandes, H.L., Empis, J. and Novais, J.M., 1996. Eicosapentaenoic Acid-Rich biomass production by the microalga *Phaeodactylum tricornutum* in a continuous-flow reactor. *Bioresource Technology*, 55, pp.83–88.

Remmers, I.M., Martens, D.E., Wijffels, R.H., and Lamers, P.P., 2017. Dynamics of triacylglycerol and EPA production in *Phaeodactylum tricornutum* under nitrogen starvation at different light intensities. *PLoS ONE*, 12, article no.e0175630.

Ryckebosch, E., Bruneel, C., Termote-Verhalle, R., Goiris, K., Muylaert, K. and Foubert, I., 2014. Nutritional evaluation of microalgae oils rich in omega-3 long chain polyunsaturated fatty acids as an alternative for fish oil. *Food Chemistry*, 160, pp.393–400.

Robbins, A., 2016. How to understand the results of the climate change summit: Conference of Parties21 (COP21) Paris 2015. *Journal of Public Health Policy*, 37, pp.129–132.

Santos, M.M.D., Moreno-Garrido, I., Gonçalves, F., Soares, A.M., & Ribeiro, R., 2002. An in situ bioassay for estuarine environments using the microalga *Phaeodactylum tricornutum*. *Environmental Toxicology and Chemistry* 21, pp.567–574.

Sayre, R., 2010. Microalgae: The Potential for Carbon Capture. *BioScience*, 60, pp.722–727.

SECIL, G., 23/8/2017 22:25. http://www.secil-group.com/

Sharma, K.K., Schuhmann, H. and Schenk, P.M., 2012. High lipid induction in microalgae for biodiesel production. *Energies*, 5, pp.1532–1553.

Shimura, S. and Fujita, Y., 1975. Changes in the activity of fucoxanthin-excited photosynthesis in the marine diatom *Phaeodactylum tricornutum* grown under different culture conditions. *Marine Biology*, 33, pp.185–194.

Silva, J.L., Marques, A., Barros, A., Campos, J., Mendonça, S.H. and Gomes, R., 2017. ALGAFARM: cultivo de microalgas à escala industrial. *TecnoAlimentar*, 12 pp.56–58.

Singh, U.B. & Ahluwalia, A.S., 2013. Microalgae: A promising tool for carbon sequestration. *Mitigation and Adaptation Strategies for Global Change*, 18, pp.73–95

Siron, R., Giusti, G. & Berland, B., 1989. Changes in the fatty acid composition of Phaeodactylum tricornutum and Dunaliella tertiolecta during growth and under phosphorus deficiency. Marine Ecology Progress Series, 55, pp.95–100.

Sobczuk, T.M., Camacho, F.G., Rubio, F.C., Fernández, F.G. and Grima, E.M., 2000. Carbon dioxide uptake efficiency by outdoor microalgal cultures in tubular airlift photobioreactors. *Biotechnology and bioengineering*, 67, pp.465-475.

Stickney, A., 1964. Salinity, Temperature, and Food Requirements of Soft-Shell Clam Larvae in Laboratory Culture. Ecological Society of America, 45(2), pp.283–291.

Swanson, D., Block, R. and Mousa, S.A., 2012. Omega-3 fatty acids EPA and DHA: health benefits throughout life. *Advances in Nutrition: An International Review Journal*, 3, pp.1–7.

Taucher, J., Jones, J., James, A., Brzezinski, M.A., Carlson, C.A., Riebesell, U. and Passow, U., 2015. Combined effects of CO 2 and temperature on carbon uptake and partitioning by the marine diatoms *Thalassiosira weissflogii* and *Dactyliosolen fragilissimus*. *Limnology and Oceanography*, 60, pp.901-919.

Thaulow, N. and Sahu, S., 2004. Mechanism of concrete deterioration due to salt crystallization. *Materials Characterization*, 53, pp.123–127.

Thornton, D.C.O., 2014. Dissolved organic matter (DOM) release by phytoplankton in the contemporary and future ocean. *European Journal of Phycology*, 49, pp.20–46.

Tredici, M.R., 2010. Photobiology of microalgae mass cultures: understanding the tools for the next green revolution. Biofuels, 1, pp.143–162.

Valenzuela, J., Mazurie, A., Carlson, R.P., Gerlach, R., Cooksey, K.E., Peyton, B.M., and Fields, M.W., 2012. Potential role of multiple carbon fixation pathways during lipid accumulation in *Phaeodactylum tricornutum*. 5, article no 40.

Vanier, G., Hempel, F., Chan, P., Rodamer, M., Vaudry, D., Maier, U.G., Lerouge, P. and Bardor, M., 2015. Biochemical characterization of human anti-hepatitis B

monoclonal antibody produced in the microalgae *Phaeodactylum tricornutum*. *PLoS ONE*, 10, article no.e0139282.

Waters, C.N., Zalasiewicz, J., Summerhayes, C., Barnosky, A.D., Poirier, C., Gałuszka, A., Cearreta, A., Edgeworth, M., Ellis,E.C., Ellis, M., Jeandel, C., Leinfelder, R., McNeill, J.R., Richter, D.B., Steffen, W., Syvitski, J., Vidas, D., Wagreich, M., Williams, M., Zhisheng, A., Grinevald, J., Odada, E., Oreskes, N. and Wolfe, A.P., 2016. The Anthropocene is functionally and stratigraphically distinct from the Holocene. *Science*, 351, pp.137–148.

Weiss, R.F., 1974. Carbon dioxide in water and seawater: the solubility of a non-ideal gas. *Marine Chemistry*, 2, pp.203–215.

Wen, Z.Y. and Chen, F., 2003. Heterotrophic production of eicosapentaenoic acid by microalgae. *Biotechnology advances*, 21, pp.273–294.

Willis, A., Chiovitti, A., Dugdale, T.M., and Wetherbee, R., 2013. Characterization of the extracellular matrix of *Phaeodactylum tricornutum* (Bacillariophyceae): structure, composition and adhesive characteristics. *Journal of Phycology*, 49, pp.937–949.

Yongmanitchai, W. and Ward, P., 1991. Growth of and omega-3 fatty acid production by *Phaeodactylum tricornutum* under different culture conditions. *Applied and Environmental Microbiology*, 57, pp.419–425.

Zhao, P., Gu, W., Wu, S., Huang, A., He, L., Xie, X., Gao, S., Zhang, B., Niu, J., Lin, A.P. and Wang, G., 2014. Silicon enhances the growth of *Phaeodactylum tricornutum* Bohlin under green light and low temperature. *Scientific reports*, 4, article no.3958

Appendix

A. Morphologies of *P. tricornutum*

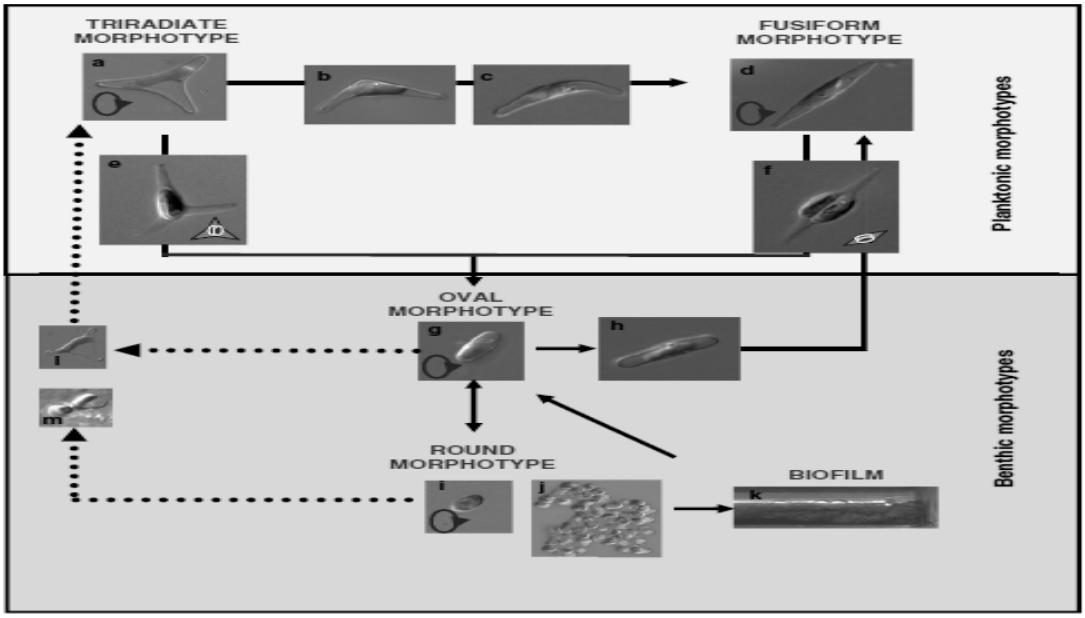

Figure a - Interaction between the morphologies of *P. tricornutum* (from: De Martino et al. 2011)

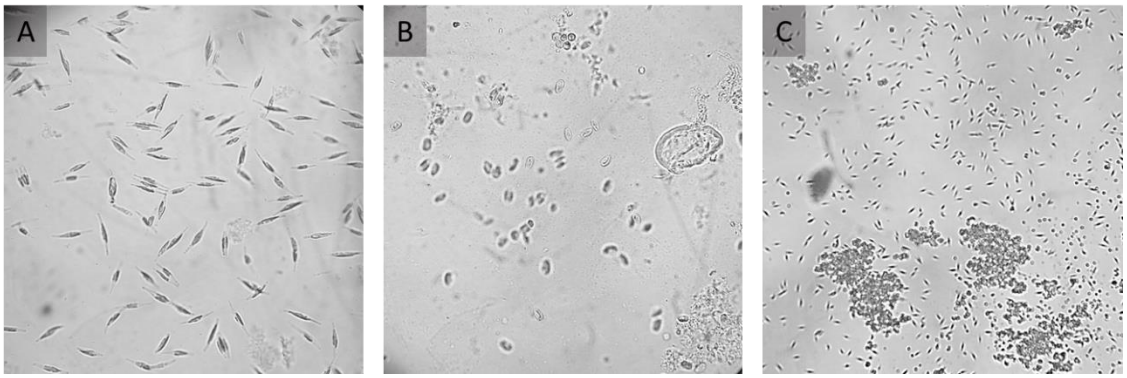

Figure b – Morphologies of *P. tricornutum* observed on optical microscopic from daily samples. A is a culture with high percentage of fusiform cells, B is a sample with a high percentage of round cells and C is a sample from a culture with clusters of round cells and fusiform in planktonic condition.

B. Calibration curves

The calibration curve of optical density versus dry weight was obtained using experimental points from daily analyses in the period between 15/2/2017 and 15/8/2017 (Figure c). It is of high importance to note that the determined correlation is only valid in the range of values presented.

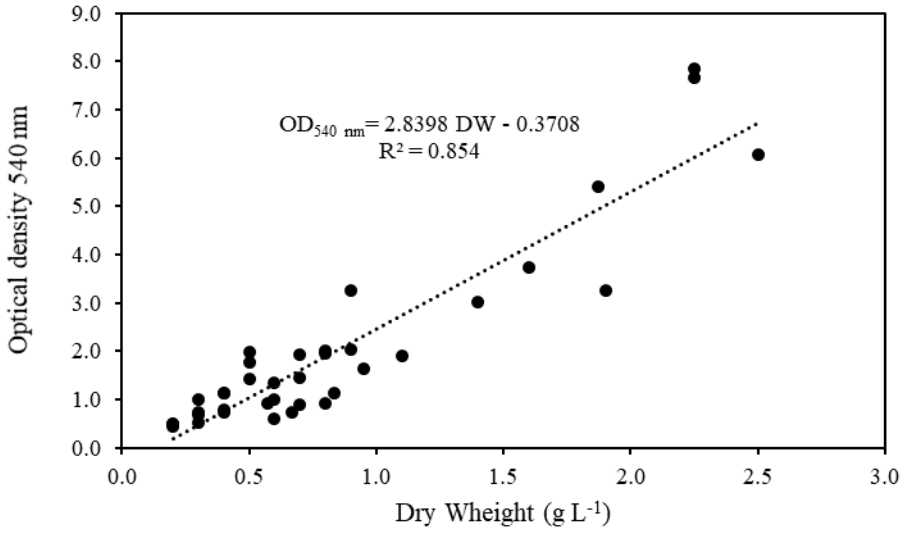

Figure c - Calibration curve of optical density at 540 nm versus dry weight of biomass culture

The calibration curve of Nephelometric Turbidity Unity (NTU) versus dry weight was obtained using experimental points from daily analyses in the period between 15/5/2017 and 15/8/2017 (Figure d). This calibration curve enables to estimate biomass concentration in dry weight throughout each day of the study.

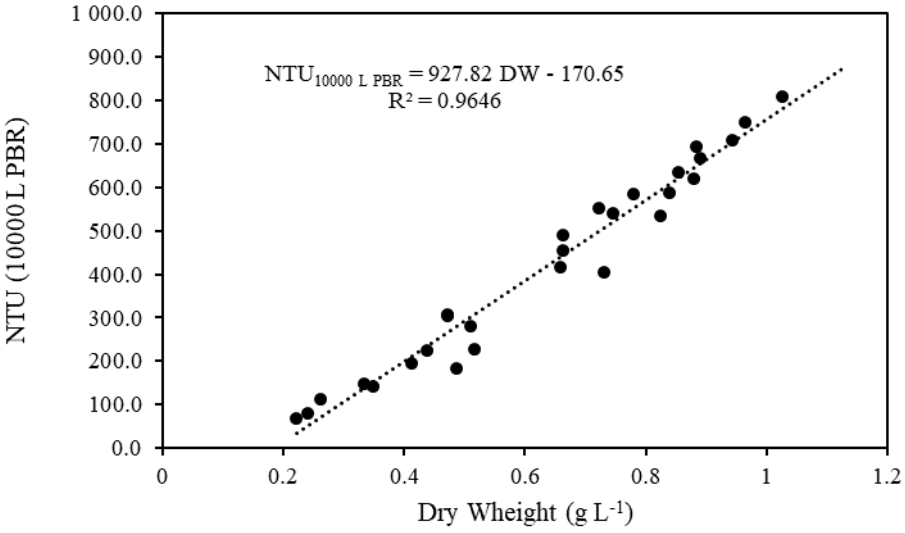

Figure d - Calibration curve of NTU in 10000 L PBR versus dry weight of biomass culture.

The calibration curve of NTU versus dry weight was obtained using experimental points from daily analyses of 35000 L PBR in the period between 1/6/2017 and 15/8/2017 (Figure e). The small differences of geometry of industrial PBR caused by scaling up, small differences of flow of culture volume and differences of turbidity probe calibration result in differences in NTU reading for a given cell concentration.

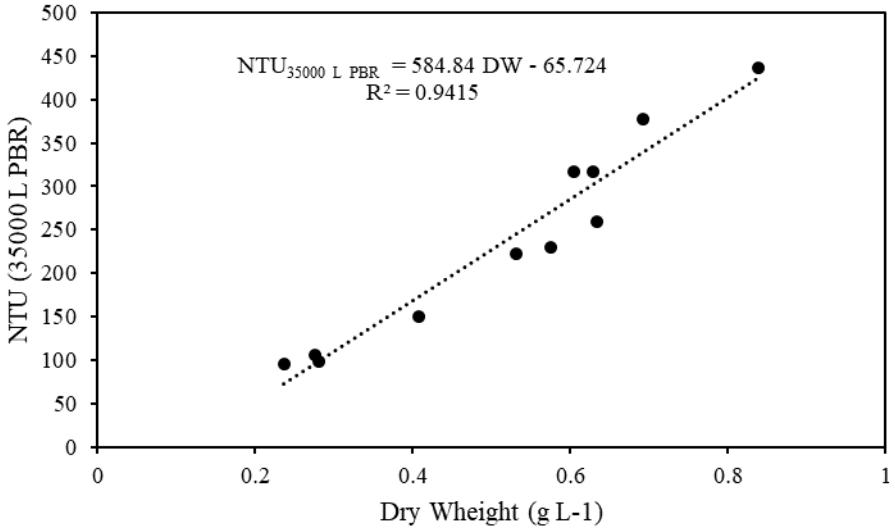

Figure e - Calibration curve of NTU in 35000 L PBR versus dry weight of biomass culture.

C. Industrial batch data

On the figure f B it is shown the growth profile with turbity reading every 20 minutes. These data evidence the loss of biomass over the night period.

The decrease on 11th and 22st days of culture corresponds to the start of a new batch.

The temperature of culture exceeded the 28ºC only for short periods of time (Figure f A - dash line).

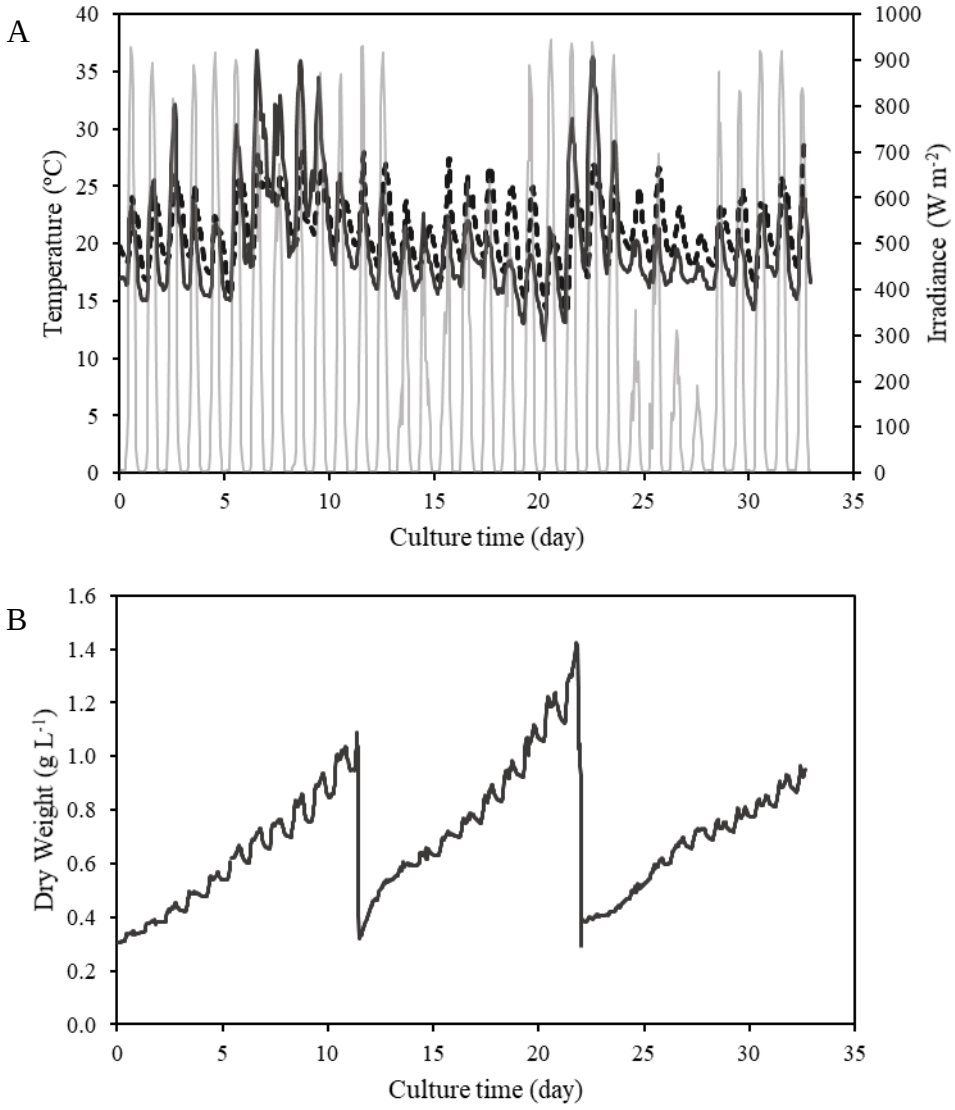

Figure f - 10000 L PBR batch data, Figure A with the temperature inside the PBR a dash dark line, temperature outside the PBR at dark grey line and a light grey line was the irradiance during all the batches. Figure B is the estimated dry weight during culture time of batches.

On the figure e B it is shown the grown profil with turbity readiging every 20 minutes. The decrease on 10th day of culture was started a new batch.

The temperature of culture exceeded 28ºC in three sucessive days (Figure g A - dash line). Although it had no serious damage on biomass and without morphological consequences.

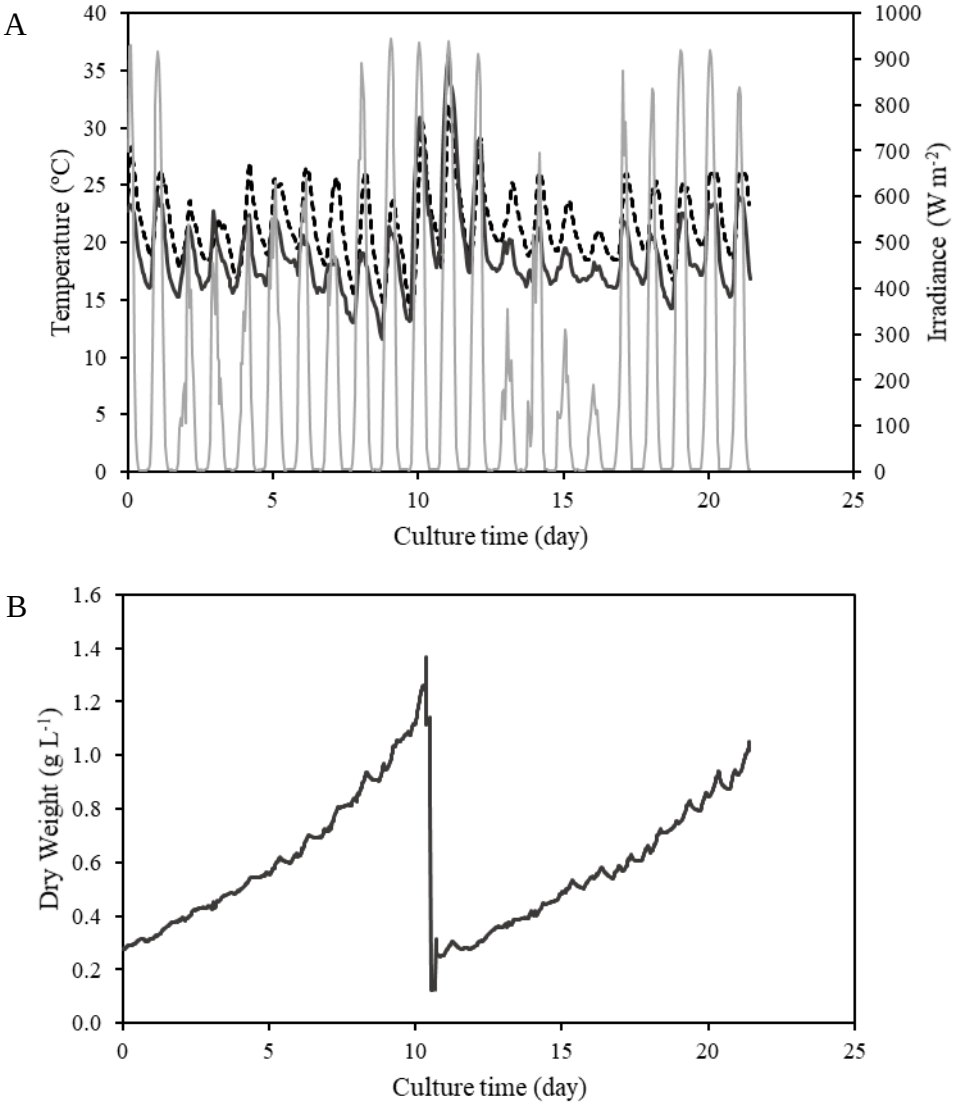

Figure g - 35000 L PBR batch data, Figure A with the temperature inside the PBR a dash dark line, temperature outside the PBR at dark grey line and a light grey line was the irradiance during both batches. Figure B is the estimated dry weight during culture time of batches.